Molecular Biosystems

Volume 1 | Number 1 | Jan 2013 | Pages 1–100

www.rsc.org/molecularbiosystems

THE BIOLOGY OF PLAGUE

ROYAL SOCIETY OF CHEMISTRY

This is an *Accepted Manuscript*, which has been through the Royal Society of Chemistry peer review process and has been accepted for publication.

Accepted Manuscripts are published online shortly after acceptance, before technical editing, formatting and proof reading. Using this free service, authors can make their results available to the community, in citable form, before we publish the edited article. We will replace this *Accepted Manuscript* with the edited and formatted *Advance Article* as soon as it is available.

You can find more information about *Accepted Manuscripts* in the **Information for Authors**.

Please note that technical editing may introduce minor changes to the text and/or graphics, which may alter content. The journal's standard **Terms & Conditions** and the **Ethical guidelines** still apply. In no event shall the Royal Society of Chemistry be held responsible for any errors or omissions in this *Accepted Manuscript* or any consequences arising from the use of any information it contains.

www.rsc.org/molecularbiosystems

1　**Elucidating time-dependent changes in urinary metabolome of renal transplant**

2　**patients by a combined ^{1}H NMR and GC-MS approach.**

3　Muhrez Kienana[a], Nadal-Desbarats Lydie[b,c] , Halimi Jean-Michel[a,d], Dieme Binta[b], Büchler

4　Matthias[a,d], Emond Patrick[b,c], Blasco Hélène[b], Le Guellec Chantal[a].

5

6　**Affiliations**

7　[a] Cellules dendritiques, immuno-intervention et greffes, EA4245, Université François

8　Rabelais, Faculté de médecine, bâtiment Vialle, 10 Boulevard Tonnellé, 37032 Tours

9　Cedex 1 - France

10　[b] Equipe neurogénétique et neurométabolomique, INSERM U930, Université François

11　Rabelais, Faculté de médecine, bâtiment Bretonneau, 10 Boulevard Tonnellé ,37044

12　Tours Cedex 9- France

13　[c] Département d'Analyse Chimique Biologique et Médicale. PPF "Analyses des Systèmes

14　Biologiques", Université François-Rabelais, Faculté de médecine, bâtiment Bretonneau,

15　10 Boulevard Tonnellé, 37032 Tours Cedex 1- France

16　[d] Service de néphrologie-immunologie clinique, CHU, hôpital Bretonneau, 2 bis boulevard

17　Tonnellé, 37044 Tours- France

18

19　**E-mail address of each author:**

20　Muhrez Kienana (kienana.muhrez@etu.univ-tours.fr)

21　Nadal-Desbarats Lydie (lydie.nadal@univ-tours.fr)

22　Halimi Jean-Michel (halimi@med.univ-tours.fr)

23　Dieme Binta (bintdiem88@yahoo.fr)

24　Büchler Matthias (buchler@med.univ-tours.fr)

25   Emond Patrick (emond@univ-tours.fr)

26   Blasco Hélène (helene.blasco@univ-tours.fr)

27   Le Guellec Chantal (chantal.barin-leguellec@univ-tours.fr)

28

29   **Corresponding author:**

30   Chantal LE GUELLEC

31   chantal.barin-leguellec@univ-tours.fr

32   Unité de Pharmacogénétique, Laboratoire de Biochimie et de Biologie Moléculaire

33   CHU - Hôpital Bretonneau, 2 bis boulevard Tonnellé - 37044 TOURS cedex, FRANCE

34   Tel : 02-47-47-80-60

35   Fax : 02-47-47-86-13

36

37

38   **ABSTRACT**

39   Urine metabolomic profiling can identify biochemical alterations resulting from various

40   injuries affecting graft outcome after renal transplantation. Here, we aimed to describe in

41   depth the metabolite content of urines of renal transplant patients and to link it with the

42   major injury factors acting at critical stages following transplantation. Morning urine

43   samples were prospectively collected from 38 kidney transplant patients at 7 days (D7),

44   3 months (M3) and 12 months (M12) after transplantation. Twenty-five patients were

45   treated with tacrolimus (Tac) and thirteen patients with ciclosporine (CsA). ^{1}H-NMR

46   (proton nuclear magnetic resonance) and gas chromatography-mass spectrometry (GC-

47   MS) were used to examine the overall metabolomic signature of each sample.

48   Multivariate analysis was performed to study changes of the metabolic profile over time

49   and their dependency on the type of calcineurin inhibitor (CNI) administered to patients.

50   Biological pathways affected by transplantation were identified by metabolomics pathway

51   analysis (MetPA) web-tool. The metabolic profile of urine samples clearly varied with

52   time. Markers of medullary injury, tubule cell oxidative metabolism and impaired tubular

53   reabsorption or secretion were present at D7. Differences in metabolic profiles became

54   less marked as time passed on, urine content being quite similar at M3 and M12. The

55   metabolite profile tended to differ between patients receiving Tac and those receiving

56   CsA but no clear discriminating profiles can be found. The combination of ^{1}H-NMR and

57   GC-MS for the analysis of urine metabolomic profiles is a very useful method to study

58   patho-physiological alterations in kidney transplant patients over time.

59

60   ***Keywords***: urinary metabolomics, calcineurin inhibitors, renal transplantation,

61   biomarkers, kidney transplant patients.

62

63   1-**INTRODUCTION**

64   Metabolite profiling is used to investigate changes of many biochemical products or

65   metabolites in biofluids (1, 2).The metabolome (the sum of all metabolites in an

66   organism) is a very sensitive measure of an organism's phenotype because metabolites

67   are the downstream products of numerous genome-wide or proteome-wide interactions

68   (3, 4). Urine contains many compounds extracted from the bloodstream or generated by

69   kidney cells themselves (5). Given the extensive knowledge of the biochemical pathways

70   of kidney metabolism, analysis of the urine metabolome in kidney transplant recipients

71   may provide information about the mechanisms involved in graft outcome, including

72   ischemia-reperfusion injury, allogenic response or immunosuppressant nephrotoxicity (6-

73   8). Metabolomics has already been applied to animals to study the consequences of

74   ischemia/reperfusion (I/R) injury (9, 10) or calcineurin inhibitor (CNI)-induced

75   nephrotoxicity (11-16). However, few studies have been conducted in humans to monitor

76   graft function after transplantation (17-19) or to study the relationship between the

77   metabolome and relevant clinical outcomes such as acute rejection (20, 21) or delayed

78   graft function (22). These, studies have examined the potential of metabolomics as a

79   source of predictive or prognostic biomarkers to optimize patient management, but none

80   have attempted to interpret biochemical changes with respect to pathophysiological

81   mechanisms, and to integrate them over time.

82   Experimental studies in animals are very useful to explore the biochemical alterations

83   resulting from a given intervention. For example, some metabolites are produced in

84   excess following the exposure of the kidneys to ischemia (I) or ischemia followed by

85   reperfusion (I/R) in animals not receiving any immunosuppressant drug (23). These

86   metabolites are thought to be produced in response to increased glycolysis (following I

87   alone) or oxidative stress (following I/R) (10). Similarly, studies investigating changes in

88   the metabolome of animals (11) or healthy volunteers (14) receiving calcineurin

89   inhibitors (CNIs) have revealed the pharmaco/toxicological effects of CNIs, with no

90   interference from ischemia/reperfusion, alloimmune response, or any other confounding

4

91   factor (14-16). Metabolomic alterations are probably very complex in human renal

92   transplantation, as many mechanisms are likely to coexist and probably show differential

93   temporal regulation.

94   We previously used gas chromatography-mass spectrometry (GC-MS) to evaluate the

95   metabolic profile of urine from patients during the first year after renal transplantation

96   (22). The aim of this initial work was to assess whether the urinary metabolome varied in

97   renal transplant patients, and whether a particular fingerprint could be identified and

98   used as a potential biomarker of early graft function. We showed that metabolomic

99   fingerprints could indeed differentiate patients according to their early renal function. The

100   metabolomic profile of urine samples varied over time, but the biological significance of

101   changes to these metabolites was not investigated due to incomplete compound

102   identification. Thus, we considered that an in depth-analysis of the urinary content

103   combining 2 analytical methods would help moving forward, particularly to elucidate the

104   biochemical pathways that are modulated in kidney grafts.

105   Although each analytical method for the analysis of the metabolome has clear

106   advantages, no single metabolomic technique can provide adequate coverage of the

107   entire human metabolome (24). Differences in terms of sensitivity, separation and/or

108   extraction efficiency mostly explain the poor overlap of metabolites isolated with each

109   method (5, 25, 26). In their comprehensive quantitative metabolome-wide

110   characterization of human urine, Bouatra et al. showed that the combined use of several

111   metabolomic techniques substantially improves the coverage of the metabolome (5).

112   From this study, it appears that urine NMR spectra are very information-rich, with

113   thousands of resolved peaks. GC-MS methods employing polar solvent extraction and

114   derivatization also achieve broad metabolite coverage. In terms of platform overlap and

115   compound complementarities, NMR and GC-MS (as a result of 4 different analyses

116   performed on 2 different GC-MS instruments) were able to identify a common set of 88

117   metabolites. Of note, NMR was able to detect 121 compounds which remained

118   undetectable using 4 different GC-MS methods whereas the combined GC-MS methods

119   detected 91 compounds undetectable using NMR. Therefore, we applied GC-MS and 1H-

120   NMR to obtain a comprehensive description of the variation over time of the urinary

121   metabolome in patients receiving a triple immunosuppressive regimen. We also carried

122   out a functional analysis of our metabolomic data to identify the specific cellular

123   processes that are altered, and their predominance at each stage or under a given

124   treatment (CNI type). The identification of these pathways will facilitate the selection and

125   prioritization of therapeutic measures in kidney transplant recipients.

126

127   **2- EXPERIMENTAL SECTION**

128   ***2.1. Patients and samples***

129   The study was carried out in compliance with the provisions of the Declaration of Helsinki

130   and the Good Clinical Practice Guidelines. All the patients gave their consent for the

131   collection and the use of the urinary data which are part of the standard care protocol

132   approved by the local ethics committee Comité de Protection des Personnes (CPP), CPP

133   de Tours Ouest-1, registered at the US department of Health and Human Services (HHS)

134   as an Institutional Review board (IRB) -(IORG0008143 OMB No. 0990-0279). Thirty-

135   eight patients were included. All patients received a cadaver kidney. The median (range)

136   cold ischemia duration was 1020 (520-1960) minutes. They received induction therapy

137   with anti-thymocyte globulin (Thymoglobulin®, Amgen, Lyon, France) or interleukin-2-

138   receptor antagonist (basiliximab, Simulect®, Novartis, Rueil-Malmaison France) and

139   maintenance immunosuppression with oral mycophenolate mofetil, a calcineurin inhibitor

140   (CNI, either cyclosporine (CsA, n=13) or tacrolimus (Tac, n=25)), and prednisone.

141   Mycophenolate mofetil was given at a dose of 1000 mg twice daily on the day of surgery,

142   and subsequently adjusted according to clinical and haematological parameters.

143   Tacrolimus was initiated on day 3 at a dose of 0.1 mg/kg twice daily, targeting a blood

144   trough concentration of 8–15 ng/mL. Cyclosporine was given at an initial dose of 8 mg

145   $kg^{-1}\ day^{-1}$, if serum creatinine was <250 µmol l^{-1}. The dose of cyclosporine was

146   individually adjusted to reach trough concentrations of 150–250 ng ml^{-1}. Target blood

Molecular BioSystems Accepted Manuscript

147 concentrations of tacrolimus and cyclosporine were progressively decreased over time.

148 Prednisone at 1 mg/kg per day for the first 2 weeks was then progressively decreased

149 and finally withdrawn within the first year after transplantation in low immunological risk

150 patients. All patients received trimethoprim-sulfamethoxazole for the first three months

151 post-transplant. CMV prophylaxis with valganciclovir at a dose of 450 mg/day, adjusted

152 for renal function, was given to all patients for the first three months after

153 transplantation except for CMV-seronegative patients who received a graft from a CMV-

154 seronegative donor. Urine samples were collected after an overnight fast in the morning

155 of the 7th day post-transplantation (D7), then at 3 months (M3) and 12 months (M12) for

156 routine measurement of proteinuria. The remaining volume was used for the

157 metabolomic study. A total of 38 urine specimens at D7 (25 Tac, 13 CsA) and 34 at M3

158 and M12 (22 Tac, 12 CsA) were collected. After centrifugation, urine supernatants were

159 stored at -20°C.

160 **2.2. Solvents and reagents**

161 All compounds and reagents used were analytical grade. Urease, N,O-Bis(trimethylsilyl)-

162 trifluoroacetamide (BSTFA) and trimethylchlorosilane (TMCS) were purchased from

163 SIGMA. Methoxyamine was from SUPELCO and methanol from Merck. Deuterium oxide

164 (D2O; 99.9%D) was purchased from Cortec Net (Paris, France).

165 **2.3. GC-MS. Sample treatment and instrumental conditions**

166 Sample treatment and instrumental conditions for GC-MS analysis were described

167 previously (22). Briefly, 200µL of urine was pretreated with urease, then mixed with

168 methanol and evaporated to dryness. The dry extract was derivatized by the addition of

169 70 µL of a mixture of BSTFA /TMCS (99/1) and 30 µL of acetonitrile for 40 min at 80 °C

170 in a sand bath. The derivatized mixture was transferred to a silanized insert for GC-MS

171 analysis. A Shimadzu GC-MS system (Kyoto, Japan) was used. This system is composed

172 of an AOC-20S auto-sampler, an AOC-20i autoinjector, a gas chromatograph 2010 and a

173 QP-2010-Plus mass spectrometer. The derivatized samples (3 µL, split ratio=10) were

174 separated on a capillary GC column (Phenomenex, Zebron ZB-5, 30 mÅ~0.25 mm i.d.,

7

175 0.25 μm film thickness). The oven temperature was set at 80 °C for 6 min, ramped to

176 300 °C at 5 °C/min and then held for 10 min. Helium was used as the carrier gas and set

177 at 0.45 mL/min. The injection port, ion source and interface temperatures were 250 °C,

178 250 °C and 300 °C, respectively. The mass spectra of all GC peaks were generated by

179 electronic impact (EI) at 70 eV and recorded in a positive total ion monitoring mode

180 scanning the 50–500m/z range (event time=0.1, scan speed=5000).

181 **2.4. 1H-NMR. Sample treatment and instrumental conditions**

182 Samples were thawed and centrifuged at 3000g for 5 min. A total of 500 μL of urine

183 supernatant was added to 100 μL of deuterium oxide (D_2O) solution. The pH was

184 adjusted to 7.4 ± 0.1 with either NaOH or HCl solution. The samples were then

185 transferred to 5-mm NMR tubes (CortecNet, Paris, France) for 1H-NMR analysis.

186 The 1H-NMR spectra were obtained with a Bruker DRX-500 spectrometer (Bruker SADIS,

187 Wissembourg, France), operating at 11.7 T, with a Broad Band Inverse (BBI) probehead

188 equipped with a Z gradient coil. NMR measurements were done at 298 °K. Conventional

189 1H-NMR spectra were recorded with a 90° pulse (p1=10 μs, pl=0 dB) using a pulse-and-

190 acquire sequence with residual water presaturation (single-frequency irradiation during

191 the relaxation delay). The 1H spectra were collected with 128 transients (and eight

192 dummy scans) in 32K data points with a spectral width of 7500 Hz, and a recycling time

193 of 30 s. Carr-Purcell-Meiboom-Gill (CPMG) spin echo spectra were obtained with 80 ms

194 total echo times and 32K data points. This spin echo sequence avoids broad short T2

195 resonance. Sample shimming was performed automatically on the water signal.

196 **2.5. Data alignment and treatment**

197 The gas chromatograms obtained were processed for smoothing, library matching and

198 area calculation using an identical data processing method created with GC-MS Solution

199 Postrun Analysis® software (Shimadzu, Japan) (Autoarea mode, maximum peak number

200 = 300, width time = 2 s, smoothing method = standard). Only peaks with minimum peak

201 area = 50 000 were selected for further analysis. The area of each peak was calculated

202 using a unique quantifier ion mass when its relative qualifier ion mass intensity was

203   within 20% range of the ratio. To minimize processing errors, each integrated peak was

204   manually checked for each sample. As recommended for the validation of GC/MS data

205   acquisition, biological quality control (QC) was performed with principal component

206   analysis (PCA) to check the validity of the data (27). The quality control (QC) sample was

207   prepared by pooling equal volumes of urine samples from all patients, from each period

208   of sampling. This QC sample was submitted to within- and between-day repeatability and

209   reproducibility analyses. In practice, for each series of GC/MS experiments, a QC sample

210   was injected on the first position, then every seven samples, and on the last position.

211   Three series of GC/MS were necessary to analyze all the samples and the experiments

212   were performed over one week. The QC sample was thus analyzed 15 times (five times

213   in each of the three chromatographic series). The QC samples were also used to identify

214   metabolites that should be excluded from data analysis because of high analytical

215   variability. Metabolites exhibiting a relative standard deviation greater than 30% in QC

216   samples were excluded in all other samples before multivariate analysis.

217   The 1H-NMR spectra were processed using XWinNMR version 3.5 software

218   (BrukerDaltonik, Karlsruhe,Germany). Prior to Fourier transformation (FT), the Free

219   Induction Decay (FID) were zero-filled to 64K data points which provided sufficient data

220   points for each resonance, and a line broadening factor of 0.3 Hz was applied. All spectra

221   were corrected for phase distortion and the baseline was manually corrected for each

222   spectrum. The 1H NMR spectra were referenced to the creatinine methylene resonance at

223   δ=4.05ppm and automatically reduced to ASCII files using the AMIX software package

224   (Analysis of MIXture, version 3.1.5, BrukerBiospin, Karslruhe, Germany). Regions

225   containing water (δ 4.70 −5.51 ppm) and urea (δ 5.58 − 6 ppm) signals were removed

226   from each spectrum to eliminate baseline effects of imperfect water saturation. Spectral

227   intensities were scaled to the total intensity and reduced to equidistant integrated

228   regions of 0.001 ppm (buckets) over the chemical shift range of 0.7-9.5 ppm. The NMR

229   spectral datasets were preprocessed using the peak alignment algorithm icoshift (28) to

230   minimize spectral peak shift due to residual pH differences within samples. The

231   corresponding realigned bucket tables were then exported to the software SIMCA-P+

232   software (version 12.0, Umetrics, Umea, Sweden) for analysis.

233   ***2.6. General flow-chart of data and statistical analysis:***

234   Each analytical tool provides a specific data table (matrix) [GC-MS (m/z and retention

235   times) and 1H-NMR (realigned bucket tables) variables]. After adequate normalization,

236   (see below), each matrix was independently submitted to multivariate analysis with

237   SIMCA P+ software (version 13.0, Umetrics, Umea, Sweden). First, unsupervised

238   principal component analysis (PCA) or supervised partial least square discriminant

239   analysis (PLS-DA) were applied to each matrix to examine patterns and trends in the

240   dataset and to detect outliers. Two-or three-dimensional score plots were used to

241   visualize the distribution of samples. Then, orthogonal projections to latent structures

242   discriminant analysis (OPLS-DA) were performed to maximize the separation between

243   classes (in our case, sampling time and CNI type) and to identify the variables

244   (metabolites obtained by either GC-MS or 1H NMR) accounting for the separation. Unit

245   variance (UV) and pareto (Par) scaling of the data were used, depending the stage of the

246   analysis. In the UV process, also known as centering, all metabolites are equally

247   important and have a comparable scale. This method was used to select the metabolites

248   from both 1H NMR and GC-MS databases. Pareto scaling is similar to UV but, after mean

249   centering, each column is divided by the square root of the standard deviation. This

250   method offers the advantage of increasing the representation of metabolites present at

251   low concentration (29, 30). It was used for the initial selection of the short-list of 1H NMR

252   metabolites.

253   S-plots, contribution plots, and variable importance on projection (VIP) values > 1 were

254   used to identify the metabolites contributing the most to the separation between classes

255   (time of sampling or CNI type). An S-plot combines the modeled covariance and the

256   modeled correlation from the OPLS-DA model in a scatter plot. The axes are plotted from

257   predictive components p[1] versus pcorr[1], representing the magnitude (modeled

258   covariance) and reliability (modeled correlation), respectively (Simca-P+ 13, Umetrics

259   Company). The coefficient plot summarizes the most important variables in the

260   separation (p(corr)[1] < 0 indicate variables associated with one group and p(corr)[1] >

261   0 variables associated with the second group). Box-plots were then constructed with

262   XLSTAT (Adinsoft, 2014) to display the difference in individual metabolite concentrations

263   between groups.

264   To determine whether the differences in metabolite profiles between sampling times (D7

265   vs M3 and D7 vs M12) were influenced by the CNI taken by the patient (Tac or CsA), the

266   prediction results (i.e. the predicted scores, scores being the new variables created by

267   weighted linear combinations of the original variables, denoted Y_{PRED}) were computed

268   with each model (models comparing D7 and M3 and D7 and M12, respectively). The Y_{PRED}

269   values for patients of Tac and CsA groups were then compared using Mann-Whitney rank

270   sum test. *P* < 0.05 was considered significant.

271   *2.6.1.Models validation*

272   Cross validation and permutation testing, two established methods of internal validation,

273   were used to confirm models validity (31-33).

274   OPLS-DA model generation employed a seven-fold cross validation step. This involves

275   omission of a portion ($1/7^{th}$) of the data from model development, development of

276   parallel models from the reduced data ($6/7^{th}$), prediction of the omitted data from the

277   different models, and then comparison of the predicted vs actual values, providing an

278   estimate of overall predictive power. The overall quality of the models was judged by the

279   cumulative R^2, defined as the proportion of variance in the data explained by the model

280   and indicating goodness of fit and by the cumulative Q^2, defined as the proportion of

281   variance in the data that can be predicted by the model thus informing about

282   predictability. Values of Q^2 and $R^2 > 0.4$ are generally considered satisfactory for

283   biological applications of metabolomics.

284   Predictive accuracy of the OPLS-DA models was summarized in terms of sensitivity and

285   specificity using receiver operating characteristics (ROC) curves generated from cross-

286   validated Y-predicted values (SIMCA-P+ software, Y-predcv, predictive Y). This tool

287   provides a quantitative measure of the performance of the model. Area under the ROC

288   curve (AUROC) was calculated using SIMCA.

289   Permutation tests involve the random assignment of class labels to cases and controls.

290   Goodness of fit and predictive ability (R^2/Q^2) of the original models must be greater than

291   those of the permuted models, or the regression line of the Q^2-points intercept must

292   cross the vertical axis at, or below zero. A hundred random permutations were performed

293   to validate the models.

294

295   *2.6.2. Specific flow-chart for 1H-NMR data*

296   Data from 1H-NMR were processed according to a semi-targeted analysis, involving pre-

297   selection of a definite number of metabolites, followed by a final analysis with these

298   metabolites only. First, a matrix containing all the buckets was created and processed

299   using Simca-P+13. Data were scaled using pareto scaling prior to OPLS-DA. S-plots were

300   then used to select a range of buckets with a VIP>1. Spectral ^{1}H assignments of these

301   features were made based on the literature values of chemical shifts in various media

302   and biofluids. A short-list of metabolites, identified from their spectra, was thus

303   generated for further multivariate analysis. Before final analysis, each selected

304   metabolite was quantified. To calculate the relative mean concentrations of the selected

305   urinary metabolites, the peak areas of the selected NMR signals of the chosen

306   metabolites were integrated using XWinNMR version 3.5 software (BrukerDaltonik,

307   Karlsruhe, Germany). The ratios of the peak areas of these selected metabolites to the

308   methylene creatinine peak (δ 4.05 ppm) were then calculated.

309   The final analysis consisted of an OPLS-DA analysis of the data matrix containing the

310   quantified metabolites, scaled to unit variance. The metabolites selected from this final

311   analysis were further submitted to univariate analysis to examine whether they each

312   contributed individually to the discrimination. SigmaStat 3.1 software (Systat Software,

313   Inc., California, USA) was used. The Mann-Whitney rank sum test was performed to

314   compare metabolite concentrations between groups, and $p < 0.05$ was considered

315   significant.

2.6.3. Specific flow-chart for GC-MS data

317   The data were processed with an untargeted analysis, i.e. all chromatographic peaks

318   were included in the multivariate analysis (22). The intensity of each ion was normalized

319   with respect to the sum of intensity of all ions detected in chromatograms to reduce both

320   the concentration differences among samples and experimental and instrumental

321   variabilities (34). This allowed generating a data matrix that consisted of metabolite

322   characteristics (retention time and m/z) and the corresponding normalized peak area

323   ("concentration"). At this step, about 500-1000 features were present in the data set.

324   Data were scaled to unit variance. OPLS-DA was applied and both coefficients and VIP

325   values were used to refine the model in a stepwise manner. A coefficient plot was used to

326   select the metabolites contributing to class separation, i.e. those showing a strong

327   correlation with the score on the predictive OPLS-DA component and with a confidence

328   interval not including the value 0. When the optimized model was obtained, the variables

329   contributing to the separation between groups were extracted from the contribution plots

330   comparing the relative abundance of each variable in each sample class (i.e. over-

331   represented or under-represented). Finally, the molecular formula of these variables was

332   identified. Metabolites from chromatographic peaks were annotated based on their MS

333   fragment patterns and retention times. The NIST05 (The National Institute of Standards

334   and Technology) library was used to identify the possible chemical formula and ionic

335   structures of the metabolites. The software proposes a list of molecules along with their

336   percentage of matching with standard compounds, indicating the most probable chemical

337   structure.

338   At this stage, two separate lists of important metabolites were obtained: one from 1H

339   NMR and another from GC-MS analyses. Overlap of metabolites between the two lists

340   was investigated, as those found in both lists would be considered the most relevant.

341   **2.7. Biological integration of the data:**

342   All the metabolites identified from the two individual matrices were analyzed

343   simultaneously with metabolomics pathway analysis (MetPA) software

344   (http://metpa.metabolomics.ca/MetPA/faces/Home.jsp), a web application designed to

345   perform pathway analysis and visualization of quantitative metabolomic data (35). This

346   tool was used to identify pathways that were deregulated in our patients. MetPA is linked

347   to the KEGG database (http://www.genome.jp/kegg-bin/show_pathway?hsa01100) and

348   metabolic pathways are presented as a network of chemical compounds with metabolites

349   as nodes and reactions as edges. The current library contains 1173 metabolic pathways

350   from 15 model organisms, including humans. When using the software, the user is asked

351   to select the particular organism in which the data were obtained. During analysis, the

352   effect of the pathway is calculated as the sum of the importance measures of the

353   matched metabolites normalized by the sum of the importance measures of all

354   metabolites in each pathway (topological analysis). Pathway enrichment analysis tests

355   whether a particular group of compounds is represented more than expected by chance

356   within the list of metabolites provided, i.e. if compounds are enriched compared to

357   random hits (Fisher's Exact test). Four compound lists were analyzed. The first one

358   included all the metabolites found in urines, whatever the sampling time. Subsequent

359   compound lists corresponded to metabolites over-represented at D7, M3 and M12,

360   respectively.

361   If needed, biological information about compounds was also retrieved from the human

362   metabolome database website (http://www.hmdb.ca) or from the literature.

363

364   **3- RESULTS**

365   ***3.1. Patient characteristics***

366   The characteristics of the patients at the time of inclusion and during follow-up are given

367   in table 1. The same number of patients received anti-lymphocyte globulins and

368   basiliximab as induction therapy in the Tac group, but basiliximab was the most

369 frequently used therapy in patients of the CsA group (92%). One patient per group

370 required dialysis after transplantation because of delayed graft function (DGF) but most

371 patients had good initial renal function. Renal function improved gradually over time in

372 both groups. At M3, a higher percentage of patients had recovered good renal function

373 (eGFR≥ 60 mL/min/1.73 m2) in the CsA group than in the Tac group (56% vs. 26%,

374 respectively) but the difference was not significant ($p=0.407$, Fisher test). At M12, all

375 patients in the CsA group, but only 31.5% of patients in the Tac group, had recovered

376 good renal function ($p=0.0004$).

377 **_3.2. Initial exploratory analysis_**

378 For both experimental approaches (GC-MS or 1H NMR), the score plots of the PCA

379 showed that the data were well separated into clusters. The samples from D7 were

380 separated from those of M12, with those at M3 lying between the two extremes. The

381 time of sampling explained part of the variability (figure 1a, 1b); 17% (second

382 component) for 1H-NMR data and 24% (first component) for GC-MS data.

383 The sampling-time classes were well separated in the 3D plots of the PLS-DA, which also

384 revealed that the CNI type contributed to intraclass variation (figure 2a, 2b).

385 **_3.3. Variation of the metabolic pattern over time_**

386 _3.3.1. 1H NMR data_

387 The short-list of metabolites, identified from the 1H NMR spectra during the first step of

388 data processing, included 17 metabolites (Figure 3). Choline, isovaleryl-glycine and lactic

389 acid were excluded of 1H NMR database because the confidence interval of these three

390 metabolites included the value 0 on the coefficient plot. After normalizing by creatinine,

391 only 16 metabolites remained (Table 2). The OPLS-DA models, built with these

392 metabolites and comparing urines from D7 and M3 and from D7 and M12, showed a

393 slight separation between D7 and M3 ($R^2X=0.164$; $Q^2=0.146$, one component only) and

394 a larger separation between D7 and M12 ($R^2X=0.275$; $Q^2=0.565$) (figure 4a, 4b).

395 Interestingly, these plots confirm that samples at each time point were also separated

396 according to the type of CNI. The two models showed good ability of classification with

397 92.6 % of samples correctly classified at D7 and 71.4 % at M3 (model D7 vs M3;

398 p<0.05) and 88.9 % of samples correctly classified at D7 and 93.1% at M12 (model D7

399 vs M12; p<0.05). Results of the permutation tests and ROC curves for these models are

400 presented in supplementary data (supplementary figure 1S and figure 2S).

401 Pairwise analysis of the contribution plots at each sampling time, i.e. D7 vs M3 and D7 vs

402 M12, enabled the identification of metabolites contributing to cluster separation (Figure

403 5). These plots indicate that concentrations of alanine, taurine, dimethylamine,

404 trimethylamine and trimethylamine N-oxide were higher at D7 than at the two later time

405 points. Succinic acid was overrepresented at D7 as compared to M12. Concentrations of

406 acetic acid, acetoacetic acid, citric acid, dihydroxyacetone, tyrosine, hippuric acid, N-

407 methyl-nicotinamide, Alpha-N-Phenylacetyl-L-Glutamine (PAG) and formic acid were

408 higher at M3 and M12 than at D7. Concentrations of N-methyl-2-pyridone-5-carboxamide

409 (2PY) were high at M3 but not at M12.

410 Univariate analysis showed that the concentration of six of these metabolites (figure 6)

411 varied significantly over time.

412 *3.3.2. GC-MS data*

413 Chromatograms of 2 different urine samples are shown in figure 7. The analysis of GC-

414 MS data also revealed a clear separation between D7 and M3 and between D7 and M12,

415 as well as between CNI types for each sampling time (figure 8a, 8b). The two models

416 showed good ability of classification with 93.3 % of samples correctly classified at D7 and

417 89.3 % at M3 (model D7 vs M3; p<0.05) and 96.3 % of samples correctly classified at

418 D7 and 86.2 % at M12 (model D7 vs M12; p<0.05). Results of the permutation tests and

419 ROC curves for these models are presented in supplementary data (supplementary figure

420 3S and figure 4S). Nine metabolites were responsible for group clustering between D7

421 and M3 and ten between D7 and M12 (Figure 5S). The list of metabolites differentially

422 represented at each sampling time is presented in table 3 (Table 3). In the absence of an

423 in-house GC-MS library, only four metabolites were formally identified. All the

424 metabolites were tested individually and their concentrations varied significantly over

425 time (Figure 6S).

426 *3.3.3. Sample normalization*

427 Sample normalization is essential to ensure sufficient homogeneity in metabolite

428 concentrations among samples for multivariate analysis (34, 36). GC-MS metabolites

429 were normalized to the total peak area, whereas 1H-NMR metabolite concentrations were

430 normalized to creatinine concentration as a measure of concentration index of urine

431 samples. Calibration to creatinine may be inadequate if creatinine production varies over

432 time or if its excretion is impacted by an external factor such as kidney impairment.

433 Thus, any time-dependent change in urinary creatinine arising from variation of kidney

434 function over time can theoretically bias the results. However, interpatient variability of

435 creatinine concentrations at each sampling period (Table 1) was much more important

436 than between-period variability (similar median value at D7, M3 or M12), indicating that

437 differences in urine dilution was much more important to consider than variation of renal

438 function and of creatinine excretion over time.

439 **3.4. Variation of the metabolite pattern according to the CNI used**

440 For both analytical methods, visual inspection of scatter plots of OPLS-DA scores

441 obtained at each sampling time appeared to show separation between patients treated

442 by CsA or by Tac (Figure 9). However, multivariate analysis failed to provide more than

443 one component and the parameters of the model were poor irrespective of the type of

444 data, NMR ($R^2X=0.36$, $Q^2=0.24$ at D7; $R^2X=0.15$, $Q^2=0.018$ at M3 and $R^2X=0.22$,

445 $Q^2=0.134$ at M12) or GC-MS ($R^2X=0.15$, $Q^2=0.17$ at D7; $R^2X=0.31$, $Q^2=0.21$ at M3 and

446 $R^2X=0.23$, $Q^2=0.022$ at M12).

447 The prediction result analysis revealed that the CNI type did not contribute significantly

448 to the separation between sampling times, either D7 vs M3 (Figure 10 a,10 b) or D7 vs

449 M12 (Figure 10 c,10 d).

450 **3.5. Biological interpretation of the data**

17

451   The 21 metabolites that showed variations in concentration at any time are shown in

452   table 4. All the metabolites identified either by ^{1}H NMR or GC-MS are included, except for

453   those that could not be formally identified (GC-MS metabolites). As a result of UV scaling

454   and of intrinsic differences in sensitivity between 1H NMR and GC-MS methods, we found

455   no overlap in the metabolites detected, at least for those that we were able to identify in

456   GC-MS.

457   Figure 11 summarizes the pathway analysis applied to all the metabolites showing

458   variations in concentration during the first year post-transplantation. This analysis

459   revealed that synthesis and degradation of ketone bodies, taurine and hypotaurine

460   metabolism, dimethylamine and methane metabolisms, dicarboxylate metabolism, citrate

461   cycle and inositol phosphate metabolism were significantly affected. Detailed results of

462   this analysis are provided in table 5, showing the more significantly enriched pathways.

463   The same analysis conducted at each sampling time revealed that inositol phosphate

464   metabolism and taurine and hypotaurine metabolism were the top pathways at D7,

465   whereas dimethylamine metabolism, pyruvate metabolism and dicarboxylate metabolism

466   had the highest effect at M3 and M12 (Table 6). Synthesis and degradation of ketone

467   bodies was the most enriched pathway at M12.

468   Finally, by combining the results from both contribution plots (individual over-

469   represented metabolites) and the metabolic pathway analysis, we were able to

470   summarize the biochemical effect of transplantation at each sampling time (Figure 12).

471

472   **4- DISCUSSION**

473   Our study shows that the composition of urinary metabolites varies over time during the

474   first year following renal transplantation. Metabolites also appeared to cluster according

475   to the type of CNI administered to patients, but we found no significant difference in

476   metabolite profiles between treatment groups. Combination of results from both

477   metabolomic analyses (individual over-represented metabolites) and metabolic pathway

478   analysis provided a general idea about the biochemical variation occurring during the first

479   year following transplantation. According to the MetPA topology of human metabolism,

480   several pathways were differentially impacted over time. For each of these pathways,

481   some of the metabolites were enriched at D7 whereas others were overrepresented at

482   later periods (figure 12).

483   In the early post-transplantation period, i.e. at D7, the main pathways affected were

484   taurine and hypotaurine metabolism (high concentrations of L-alanine and taurine),

485   dimethylamine and methane metabolism (high concentrations of dimethylamine (DMA),

486   trimethylamine (TMA) and trimethylamine N-oxide (TMAO)), citrate cycle (low

487   concentrations of citric acid), inositol phosphate metabolism (high concentrations of

488   myoinositol) and glycolysis (high concentrations of D-Glucose). To facilitate the

489   interpretation of these data, we compared our results with those from previous

490   experimental studies exploring the short-term effects of particular injuries on the kidney

491   or urinary metabolome. Ischemia-reperfusion appears to be a key mechanism in kidney

492   injury after transplantation, leading to an abrupt decline of energy supply, and

493   mitochondrial damage (8, 37). When cold ischemia is applied in isolation, there is an

494   increase in concentrations of glycogen, carbohydrate and lactate, an end-product of

495   anaerobic glycolysis (10). Following reperfusion, concentration of urinary allantoin

496   increases, suggesting oxidative stress. Hauet et al. assessed the consequences of

497   ischemia-reperfusion with various preservative solutions following auto-transplantation in

498   pigs. They reported that urinary concentrations of lactic and acetic acid increased and

499   those of citric acid decreased following reperfusion, and attributed these changes to

500   impaired oxidative metabolism in proximal cells (9). We also found that acetic acid

501   concentrations were lower at D7, but we cannot draw any conclusions about lactic acid

502   because this metabolite was excluded from our multivariate analysis as previously

503   mentioned. In our study, the concentration of citric acid was also lower at D7 than at

504   later periods. Consistent with the presence of oxidative stress, taurine, an endogenous

505   antioxidant which limits I/R injury, was present at D7.

506   Urine at D7 also contained higher concentrations of DMA, TMA and TMAO than urine at

507   M3 and M12. These metabolites, synthesized by the medullar cells of the kidney, regulate

508   osmotic flux across the cell surface membrane (9). They are not normally found in urine

509   but are released from cells exposed to medullary toxins or to ischemia-reperfusion. The

510   detection of myoinositol in urine at D7 confirms the presence of medullary injury because

511   this metabolite plays a crucial role in osmoregulation in cells of the thick ascending limb

512   of Henle (38). Thus, consistent with animal studies, we show that renal transplantation in

513   humans is associated with early renal medullary injury.

514   Collectively, our results indicate that the profile of metabolites found in renal transplant

515   patients seven days after grafting is very similar to that found in animals subjected to

516   pure ischemia-reperfusion injury (8). However, the presence of metabolites reflecting

517   mitochondrial dysfunction (citrate cycle intermediates), but also impaired tubular

518   secretion (low hippuric acid) or reabsorption (high glucose) is also suggestive of the

519   toxicodynamic metabolic effects of CNI. Schmitz et al (16) used a syngenic rat transplant

520   model to study whether CNI worsens the damage caused by ischemia/reperfusion. They

521   compared the urinary metabolic profiles of rats after ischemia-reperfusion alone or with

522   short-term co-administration of immunosuppressant drugs. At D7, concentrations of

523   metabolites related to mitochondrial energy metabolism (succinic acid, citric acid, 2-oxo-

524   glutarate) and to reactive oxygen species (creatine, taurine) were significantly different

525   between treated and untreated animals. Furthermore, the combined effects of

526   immunosuppressant and transplantation led to more proximal tubular injury (high

527   concentrations of urinary glucose, low concentrations of hippurate) than transplantation

528   alone. Several studies evaluating the isolated effects of calcineurin inhibitors in animals

529   or in healthy volunteers reached the same conclusions. All showed that CNI treatment

530   induced a decrease of citrate cycle metabolites and an increase of glucose, lactate,

531   creatine, acetic acid and TMA in urine (13-15). Interestingly, these immunosuppressant-

532   related effects were also present in our patients and overlapped with those related to

533   ischemia-reperfusion.

534

535   Thus, we conclude that the effects observed in the urine of patients at D7 are consistent

536   with those of experimental studies, and are the result of both ischemia-reperfusion-injury

537   and acute CNI toxicity. A combination of metabolites, including markers of medullary

538   injury (DMA, TMA, TMAO, myoinositol), tubule cell oxidative metabolism (citric acid, oxo-

539   glutarate, succinic acid, lactic acid, taurine), tubular reabsorption (glucose, amino-acids)

540   or secretion (hippuric acid), thus reflect the ongoing patho-physiological mechanisms

541   occurring at the early stage of human renal transplantation. The altered metabolite

542   profile seen in our patients may be related to global suppression of mitochondrial activity

543   and to decreased organic anion or cation elimination. The organic anion transporters,

544   OAT1 and OAT3 and the organic cation transporter, OCT2 are the main polyspecific

545   transporters expressed in the renal proximal tubule. These transporters are the rate-

546   limiting step in the renal uptake of various metabolites from blood (39). Thus, it is

547   possible that reduction in OAT1/3 or OCT2 activity may contribute to the reduced urinary

548   level of some of the metabolites identified. It has been shown that OATs are down

549   regulated during reperfusion after ischemic acute kidney injury (40-42). Among

550   immunosuppressive medications, mycophenolic acid can also inhibit OAT's function (43).

551

552   Our study did not identify any metabolites not previously found in studies of selective I/R

553   or CNI-induced injuries; therefore, we have no evidence to suggest that metabolomic

554   alterations arose from alloimmune responses or any of other damage occurring in the

555   immediate post-transplant period.

556

557   Our study also provides information about how metabolomic alterations change over

558   time, as revealed by both pathway analysis (Figure 12) and variation in the concentration

559   of individual metabolites (figures 6 and figure 6S). The effect of transplantation on the

560   citrate cycle varied over time (concentrations of succinic acid decreased at M12, whereas

561   those of citric acid and cis-aconitic acid increased), revealing improvement of

562   mitochondrial function. Similarly, effects related to medullary injury also changed with

563   time, as evidenced by the shift from DMA, TMA and TMAO toward other metabolites of

564   this pathway, dihydroxyacetone and formic acid. Transport function of the proximal

565   tubule also improved as shown by the decrease of glucose and the appearance of

566   hippuric acid in urine over time. Interestingly, concentrations of metabolites of the

567   ketone bodies pathway (3-hydroxybutyric acid and acetoacetic acid) increased in urine

568   from the 3rd month post-transplantation. The ketone content of urine is usually very low.

569   However, if carbohydrates cannot be used for energy, the body utilizes fat, and ketones

570   are formed as a by-product. The presence of ketones in the urine of our patients may

571   reflect poor control of their initial diabetes or could be an early sign of new onset

572   diabetes after transplantation (NODAT). We were not able to verify this hypothesis in our

573   cohort because NODAT was not systematically retrieved in the database and it mostly

574   occurs after M12.

575   Urine at M3 and M12 also contained metabolites related to nicotinamide metabolism (N-

576   methyl-2-pyridone-5-carboxamide (2PY), N-methylnicotinamide). These metabolites,

577   derived from the breakdown of NAD^+, are found in the urine of healthy individuals as a

578   result of their renal elimination. Thus, their presence in the urines at M3 and M12

579   indicates that they were better excreted than at the earlier period (D7). Renal function of

580   our patients improved at M3 and M12 as compared to D7 (Table 1). Furthermore, as N-

581   methylnicotinamide is an endogenous substrate for the organic cation transporters (45,

582   46), one can hypothesize that down-regulation of renal transporters observed in the

583   early period in response to ischemia-reperfusion has resolved at later ones. The presence

584   of these metabolites in urine may also originate from the inhibition of IMPDH (inosine

585   monophosphate deshydrogenase) by mycophenolic acid (MPA), which was administered

586   as the third immunosuppressive agent in our patients. IMPDH (IMP:NAD^+

587   oxidoreductase) catalyzes the NAD^+-dependent oxidation of IMP to xanthosine

588   monophosphate (47). Inhibition of IMPDH by MPA could cause accumulation of its

589   substrates, IMP and NAD^+, thus explaining the high level of niconinamide metabolites in

590   urine. However, NAD^+/NADH are central for energy metabolism and several factors may

591   affect their abundance.

592   Our study provides insight into the time-dependent consequences of transplantation but

593   sheds no light on the controversial issue of differential nephrotoxic effects of CsA and

594   tacrolimus. Although OPLS-DA revealed slight differences at each sampling time between

595   the urine of patients treated with Tac or CsA, the metabolite profiles, summarized by the

596   Y_{PRED}, were not significantly different. Thus, we did not identify a set of metabolites

597   indicative of CNI-specific effects. Only one study in rats has compared the urinary

598   metabolomic profile between the two drugs (48). At the doses tested, changes after

599   tacrolimus were less pronounced than those observed after treatment with cyclosporine.

600   Both drugs affected the same biochemical pathways (citric acid cycle and hippuric acid),

601   and only the magnitude of the effect on these pathways differed. However, in the only

602   study in humans to compare the two drugs, patients receiving tacrolimus exhibited

603   several specific changes that were not observed in those receiving cyclosporine.

604   However, this study reports metabolomic data in serum, which prevents comparison with

605   our results (12).

606

607   In conclusion, we provide for the first time longitudinal metabolomic data in renal

608   transplant patients. Although the factors contributing to graft outcome are

609   interdependent, the main mechanisms contributing to graft injury can be individually

610   distinguished. Thus, experimental results obtained in animals are transposable to

611   humans. Our data pave the way for the widespread implementation of pharmaco-

612   metabolomic studies that will improve our understanding of the effects of drugs and

613   facilitate the testing of new therapeutic strategies preventing kidney damage after

614   transplantation.

615

616   **CONFLICTS OF INTERESTS:**

617   None

618   **FINANCIAL SUPPORT:**

621

622

623   REFERENCES

624   1.   Forsythe I.J., Wishart D.S. Exploring human metabolites using the human
625   metabolome database. *Curr Protoc Bioinformatics* 2009;Chapter 14:Unit14 8..
626   2.   Frolkis A., Knox C., Lim E., et al. SMPDB: The Small Molecule Pathway Database.
627   *Nucleic Acids Res* 2010;38(Database issue):D480-7..
628   3.   Abu Bakar M.H., Sarmidi M.R., Cheng K.K., et al. Metabolomics - the
629   complementary field in systems biology: a review on obesity and type 2 diabetes. *Mol*
630   *Biosyst* 2015..
631   4.   Patel S., Ahmed S. Emerging field of metabolomics: big promise for cancer
632   biomarker identification and drug discovery. *J Pharm Biomed Anal* 2015;107:63-74..
633   5.   Bouatra S., Aziat F., Mandal R., et al. The human urine metabolome. *PLoS One*
634   2013;8(9):e73076..
635   6.   Niemann C.U., Serkova N.J. Biochemical mechanisms of nephrotoxicity:
636   application for metabolomics. *Expert Opin Drug Metab Toxicol* 2007;3(4):527-44..
637   7.   Blydt-Hansen T.D., Sharma A., Gibson I.W., Mandal R., Wishart D.S. Urinary
638   metabolomics for noninvasive detection of borderline and acute T cell-mediated rejection
639   in children after kidney transplantation. *Am J Transplant* 2015;14(10):2339-49..
640   8.   Wei Q., Xiao X., Fogle P., Dong Z. Changes in metabolic profiles during acute
641   kidney injury and recovery following ischemia/reperfusion. *PLoS One*
642   2014;9(9):e106647..
643   9.   Hauet T., Baumert H., Gibelin H., et al. Noninvasive monitoring of citrate, acetate,
644   lactate, and renal medullary osmolyte excretion in urine as biomarkers of exposure to
645   ischemic reperfusion injury. *Cryobiology* 2000;41(4):280-91..
646   10.   Serkova N., Fuller T.F., Klawitter J., Freise C.E., Niemann C.U. H-NMR-based
647   metabolic signatures of mild and severe ischemia/reperfusion injury in rat kidney
648   transplants. *Kidney Int* 2005;67(3):1142-51..
649   11.   Bohra R., Schoning W., Klawitter J., et al. Everolimus and sirolimus in combination
650   with cyclosporine have different effects on renal metabolism in the rat. *PLoS One*
651   2012;7(10):e48063..
652   12.   Kim C.D., Kim E.Y., Yoo H., et al. Metabonomic analysis of serum metabolites in
653   kidney transplant recipients with cyclosporine A- or tacrolimus-based
654   immunosuppression. *Transplantation* 2010;90(7):748-56..
655   13.   Klawitter J., Bendrick-Peart J., Rudolph B., et al. Urine metabolites reflect time-
656   dependent effects of cyclosporine and sirolimus on rat kidney function. *Chem Res Toxicol*
657   2009;22(1):118-28..
658   14.   Klawitter J., Haschke M., Kahle C., et al. Toxicodynamic effects of ciclosporin are
659   reflected by metabolite profiles in the urine of healthy individuals after a single dose. *Br J*
660   *Clin Pharmacol* 2010;70(2):241-51..
661   15.   Lenz E.M., Bright J., Knight R., Wilson I.D., Major H. Cyclosporin A-induced
662   changes in endogenous metabolites in rat urine: a metabonomic investigation using high
663   field 1H NMR spectroscopy, HPLC-TOF/MS and chemometrics. *J Pharm Biomed Anal*
664   2004;35(3):599-608..
665   16.   Schmitz V., Klawitter J., Bendrick-Peart J., et al. Metabolic profiles in urine reflect
666   nephrotoxicity of sirolimus and cyclosporine following rat kidney transplantation. *Nephron*
667   *Exp Nephrol* 2009;111(4):e80-91..
668   17.   Calderisi M., Vivi A., Mlynarz P., et al. Using metabolomics to monitor kidney
669   transplantation patients by means of clustering to spot anomalous patient behavior.
670   *Transplant Proc* 2013;45(4):1511-5..
671   18.   Wang J., Zhou Y., Xu M., Rong R., Guo Y., Zhu T. Urinary metabolomics in
672   monitoring acute tubular injury of renal allografts: a preliminary report. *Transplant Proc*
673   2011;43(10):3738-42..
674   19.   Li L., Sui W., Che W., et al. 1H NMR-based metabolic profiling of human serum
675   before and after renal transplantation. *Asaio J* 2013;59(3):286-93..
676   20.   Chen J., Wen H., Liu J., et al. Metabonomics study of the acute graft rejection in
677   rat renal transplantation using reversed-phase liquid chromatography and hydrophilic

678   interaction chromatography coupled with mass spectrometry. *Mol Biosyst*
679   2012;8(3):871-8..
680   21.   Zhao X., Chen J., Ye L., Xu G. Serum Metabolomics Study of the Acute Graft
681   Rejection in Human Renal Transplantation Based on Liquid Chromatography-Mass
682   Spectrometry. *J Proteome Res* 2014..
683   22.   Dieme B., Halimi J.M., Emond P., et al. Assessing the Metabolic Effects of
684   Calcineurin Inhibitors in Renal Transplant Recipients by Urine Metabolic Profiling.
685   *Transplantation* 2014..
686   23.   Chouchani E.T., Pell V.R., Gaude E., et al. Ischaemic accumulation of succinate
687   controls reperfusion injury through mitochondrial ROS. *Nature* 2014;515(7527):431-5..
688   24.   Williams R., Lenz E.M., Wilson A.J., et al. A multi-analytical platform approach to
689   the metabonomic analysis of plasma from normal and Zucker (fa/fa) obese rats. *Mol
690   Biosyst* 2006;2(3-4):174-83..
691   25.   Chen J.J., Liu Z., Fan S.H., et al. Combined application of NMR- and GC-MS-based
692   metabonomics yields a superior urinary biomarker panel for bipolar disorder. *Sci Rep*
693   2014;4:5855..
694   26.   Law W.S., Huang P.Y., Ong E.S., et al. Metabonomics investigation of human urine
695   after ingestion of green tea with gas chromatography/mass spectrometry, liquid
696   chromatography/mass spectrometry and (1)H NMR spectroscopy. *Rapid Commun Mass
697   Spectrom* 2008;22(16):2436-46..
698   27.   Hu J.D., Tang H.Q., Zhang Q., et al. Prediction of gastric cancer metastasis
699   through urinary metabolomic investigation using GC/MS. *World J Gastroenterol*
700   2011;17(6):727-34..
701   28.   Savorani F., Tomasi G., Engelsen S.B. icoshift: A versatile tool for the rapid
702   alignment of 1D NMR spectra. *J Magn Reson* 2010;202(2):190-202..
703   29.   Gromski P., Xu Y., Hollywood K., Turner M., Goodacre R. The influence of scaling
704   metabolomics data on model classification accuracy. *Metabolomics* 2015;11:684-95..
705   30.   Van Den Berg R.A., Hoefsloot H.C., Westerhuis J.A., Smilde A.K., Van Der Werf
706   M.J. Centering, scaling, and transformations: improving the biological information
707   content of metabolomics data. *BMC Genomics* 2006;7:142..
708   31.   Eriksson L., Johansson E., Kettaneth-Wold N., Trygg J., Wilkstrom C., Wold S.
709   Multivariate and megavariate data analysis advanced applications and extensions (Part I
710   and II). Umea, Sweeden: Umetrics, INC.; 2006..
711   32.   Hastie T., Tibshirani R., Friedman J. The elements of statistical learning: data
712   mining, inference and predistion: with 200 full-color illustrations. New-York: Springer;
713   2001..
714   33.   Pesarin F. Multivariate permutation tests: With apllication in biostatistics.
715   Chichester, New-York: Wiley; 2001..
716   34.   Chen Y., Shen G., Zhang R., et al. Combination of injection volume calibration by
717   creatinine and MS signals' normalization to overcome urine variability in LC-MS-based
718   metabolomics studies. *Anal Chem* 2013;85(16):7659-65..
719   35.   Xia J., Mandal R., Sinelnikov I.V., Broadhurst D., Wishart D.S. MetaboAnalyst 2.0-
720   -a comprehensive server for metabolomic data analysis. *Nucleic Acids Res* 2012;40(Web
721   Server issue):W127-33..
722   36.   Warrack B.M., Hnatyshyn S., Ott K.H., et al. Normalization strategies for
723   metabonomic analysis of urine samples. *J Chromatogr B Analyt Technol Biomed Life Sci*
724   2009;877(5-6):547-52..
725   37.   Murphy M.P. How mitochondria produce reactive oxygen species. *Biochem J*
726   2009;417(1):1-13..
727   38.   Kitamura H., Yamauchi A., Sugiura T., et al. Inhibition of myo-inositol transport
728   causes acute renal failure with selective medullary injury in the rat. *Kidney Int*
729   1998;53(1):146-53..
730   39.   Hediger M.A., Clemencon B., Burrier R.E., Bruford E.A. The ABCs of membrane
731   transporters in health and disease (SLC series): introduction. *Mol Aspects Med*
732   2013;34(2-3):95-107..

733 40. Bischoff A., Bucher M., Gekle M., Sauvant C. PAH clearance after renal ischemia
734 and reperfusion is a function of impaired expression of basolateral Oat1 and Oat3. *Physiol*
735 *Rep* 2014;2(2):e00243..
736 41. Di Giusto G., Anzai N., Endou H., Torres A.M. Elimination of organic anions in
737 response to an early stage of renal ischemia-reperfusion in the rat: role of basolateral
738 plasma membrane transporters and cortical renal blood flow. *Pharmacology*
739 2008;81(2):127-36..
740 42. Matsuzaki T., Watanabe H., Yoshitome K., et al. Downregulation of organic anion
741 transporters in rat kidney under ischemia/reperfusion-induced acute [corrected] renal
742 failure. *Kidney Int* 2007;71(6):539-47..
743 43. El-Sheikh A.A., Greupink R., Wortelboer H.M., et al. Interaction of
744 immunosuppressive drugs with human organic anion transporter (OAT) 1 and OAT3, and
745 multidrug resistance-associated protein (MRP) 2 and MRP4. *Transl Res* 2013;162(6):398-
746 409..
747 44. Schneider R., Meusel M., Betz B., et al. Oat1/3 Restoration Protects against Renal
748 Damage after Ischemic AKI. *Am J Physiol Renal Physiol* 2014:ajprenal 00160 2014..
749 45. Muller F., Pontones C.A., Renner B., et al. N(1)-methylnicotinamide as an
750 endogenous probe for drug interactions by renal cation transporters: studies on the
751 metformin-trimethoprim interaction. *Eur J Clin Pharmacol* 2015;71(1):85-94..
752 46. Fromm M.F. Prediction of transporter-mediated drug-drug interactions using
753 endogenous compounds. *Clin Pharmacol Ther* 2012;92(5):546-8..
754 47. Fleming M.A., Chambers S.P., Connelly P.R., et al. Inhibition of IMPDH by
755 mycophenolic acid: dissection of forward and reverse pathways using capillary
756 electrophoresis. *Biochemistry* 1996;35(22):6990-7..
757 48. Klawitter J., Klawitter J., Kushner E., et al. Association of immunosuppressant-
758 induced protein changes in the rat kidney with changes in urine metabolite patterns: a
759 proteo-metabonomic study. *J Proteome Res* 2010;9(2):865-75..

760

Figure legends:

Figure 1: Score plot of PCA analysis of 1H NMR (1a) and GC-MS (1b) data. Urine was

collected at D7 (Green), at M3 (Gray) and at M12 (Red). R^2Ycum and Q^2cum were

calculated from the two first components in PCA (1a:R^2X=0.427; Q^2=-0.0669 and 1b:

R^2X=0.374; Q^2=0.31).

Figure 2: 3D Score plot of PLS-DA analysis of 1H NMR (2a) and GC-MS (2b) data of urine

from patients treated with CsA (circles) or Tac (triangles) at the three sampling times,

i.e. D7 (Green), M3 (Gray) and M12 (Red). R2Ycum and Q2cum were calculated

(2a:R^2X=0.275; Q^2=0.057 and 2b:R^2X=0.321; Q^2=0.308).

Figure 3: 1H NMR spectrum of a urine sample showing dimethylamine (DMA),

trimethylamine (TMA), trimethylamine N-oxide (TMAO), alpha-N-Phenylacetyl-L-

Glutamine (PAG), N-methyl-2-pyridone-5-carboxamide (2PY) and N-methylnicotinamide

(NMNA).

Figure 4: Score plots of pairwise comparison by OPLS-DA of 1H NMR data of (a) urine at

D7 (Green dots) *vs* urine at M3 (Gray dots) (R^2X=0.164; Q^2=0.146) and of (b) urine at

D7 (Green dots) *vs* urine at M12 (Red dots) (R^2X=0.275; Q^2=0.565)

Patients treated with CsA are indicated with dotted circles whereas those treated with Tac

are indicated with continuous circles.

Figure 5: Contribution plots of 1H NMR data showing the major metabolites accounting

for the separation between (a) urine at D7 (green) and at M3 (gray) and (b) urine at D7

(green) and at M12 (red); positive values show the metabolites that are highly abundant

at M3 (5a) and M12 (5b) whereas negative values show those that are highly abundant

at D7 (5a and 5b). Alpha-N-Phenylacetyl-L-Glutamine (PAG), N-methyl-2-pyridone-5-

carboxamide (2PY), Trimethylamine (TMA), N-methylnicotinamide (NMNA),

Dimethylamine (DMA) and Trimethylamine N-oxide (TMAO).

Figure 6: Box-plots of individual metabolite/Cr ratios (1H NMR data) at the three

sampling times (D7, M3 and M12).

788   Figure 7: Chromatograms of 2 different urine samples. Metabolites in urine appear as

789   chromatographic peaks, characterized by their intensity (Y axis) and retention time (X

790   axis). The overlay view enables visualization of differences in the urinary content for each

791   metabolite.

792   Figure 8: Score plots of pairwise comparison by OPLS-DA of GC-MS data of (a) urine at

793   D7 (Green dots) vs urine at M3 (Gray dots) ($R^2X=0.54$; $Q^2=0.59$) and of (b) urine at D7

794   (Green dots) vs urine at M12 (Red dots) ($R^2X=0.64$; $Q^2=0.624$). Patients treated with

795   CsA are indicated by dotted circles whereas those treated with Tac are indicated by

796   continuous circles.

797   Figure 9: Pairwise comparison by OPLS-DA of urine from patients treated with CsA (black

798   dots) or Tac (red dots) analyzed by ^{1}H NMR at the three sampling times. (a) Comparison

799   at D7 ($R^2X=0.36$; $Q^2=0.24$), (b) Comparison at M3 ($R^2X=0.15$; $Q^2=0.018$) and (c)

800   Comparison at M12 ($R^2X=0.13$; $Q^2=0.22$).And those analyzed by GC-MS at the three

801   sampling times. (d) Comparison at D7 ($R^2X=0.15$; $Q^2=0.17$), (e) Comparison at M3

802   ($R^2X=0.31$; $Q^2=0.21$) and (f) comparison at M12 ($R^2X=0.23$; $Q^2=0.022$).

803   Figure 10: Box-plots of Y values for Tac and CsA groups, computed with the model

804   comparing D7 and M3 (10-a 1H NMR data; p value=0.501; 10-b GC-MS data; p

805   value=0.979),and those computed with the model comparing D7 and M12 (10-c ^{1}H NMR

806   data; p value=0.299;10-d GC-MS data; p value=0.276).

807   Figure 11: Summary of the pathway analysis with MetPA when all the metabolites (^{1}H

808   NMR and CG-MS), at each sampling time (D7, M3 and M12) were considered. The area of

809   the bubbles is proportional to the effect of each pathway, with color denoting the

810   significance from highest in red to lowest in white. (a) Synthesis and degradation of

811   ketone bodies, (b) Taurine and hypotaurine metabolism, (c) Dimethylamine and methane

812   metabolisms, (d) Dicarboxylate metabolism, (e) Citrate cycle, (f) Pyruvate metabolism.

813

814   Figure 12: Summary of the variation in metabolite concentration over time after kidney

815   transplantation. Metabolites are listed in rows and biochemical pathways in columns.

816   Color key indicates high concentrations of the metabolite at a given sampling time.

817

818

819

820

821

822

823

824

825

826

827

828

829

830

831

832

833

834

835

836

837

838

839

840

841

842

843

844

845

846

847

848

849

850

851

852

853

854

855

856

857

858

859

Table I: Patient characteristics

Characteristics	Tac group	CsA group
Baseline characteristics of all patients		
Males/females	15 / 10	7 / 6
Age median (range), years	59 (16- 74)	50 (20- 67)
Weight median (range), kg	73 (40 - 105)	75 (59 - 111)
Characteristics of patients analyzed at D7		
Creatininemia median (range), µmol/L	195 (92 - 1490)	146 (80 - 464)
Creatininuria median (range), mmol/L	4.44 (1.02-9.04)	4.69 (1.42-7.32)
Proteinuria median (range), g/L	0.51 (0.09-1.98)	0.39 (0.12-1.24)
Characteristics of patients analyzed at M3		
Creatininemia median (range), µmol/L	137 (78 - 369)	133 (77 - 206)
Creatininuria median (range), mmol/L	3.48 (0.95-11.76)	4.15 (2.73-6.34)
Proteinuria median (range), g/L	0.09 (0-0.32)	0.07 (0-1.68)
eGFR median (range), mL/min/1.73 m2	54 (17.5 - 105)	55 (48.3 - 106)
Characteristics of patients analyzed at M12		
Creatininemia median (range), µmol/L	129 (89 - 356)	109 (82 - 171)
Creatininuria median (range), mmol/L	5.19 (1.43-11.61)	5.5 (1.54-10.56)
Proteinuria median (range), g/L	0.11 (0-0.53)	0.06 (0-0.52)
eGFR median (range), mL/min/1.73 m2	48 (14.7 - 115)	70 (63 - 118)

Tac :Tacrolimus,   CsA :Cyclosporine

860

861

862

863

864

Table 2: Metabolites that were identified in urines of patients By 1H NMR

Compound	chemical shift (ppm)
L-Alanine	1.48 (d)
Acetic acid	1.93 (s)
Acetoacetic acid	2.34 (s)
Succinic acid	2.42 (s)
Citric acid	2.63 (d) , 2.69 (d)
Dimethylamine	2.72 (s)
Trimethylamine	2.86 (s)
Taurine	3.25 (t) , 3.41 (t)
Trimethylamine N-oxide	3.27 (s)
Dihydroxyacetone	4.45 (s)
Tyrosine	6.87 (d) , 7.13 (d)
Alpha-N-Phenylacetyl-L-Glutamine	7.35 - 7.46 (tt)
Hippuric acid	7.54 (m), 7.63 (m), 7.83 (m)
N-methyl-2-pyridone-5-carboxamide (2PY)	8.27 (s) , 8.33 (d)
Formic acid	8.46 (s)
N-methylnicotinamide	8.84 (t) , 9.1 (s)

ppm : One part per million (ppm)

(s): singlet , (d):doublet , (t): triplet , (m):multiplet

865

866

867

868

869

870

871

Table 3: Metabolites differing between D7 and M3 or M12 in urines of patients treated with Tac or CsA

Model	Feature	VIP	Retention time (min)	p	Content variance	Proposed identification	Percentage match (%)
D7 vs M3							
	M217T1046	1,211	17,43	<0.0001	↑ D7	Myo-inositol	89%
	M42T443	1,095	7,38	<0.0001	↑ D7	Characterized by the ions 57,100,70,144,188,203	
	M254T678	1,04	11,3	0,001	↑ M3	Characterized by the ions 254;284;299	
	M282T838	1,028	13,96	0	↑ D7	?	
	M157T946	0,996	15,76	0	↑ D7	D-Glucose	91%
	M199T1565	0,921	26,08	0,004	↑ D7	?	
	M160T925	0,914	15,4	0	↑ D7	D-Glucose (?)	84%
	M189T823	0,877	13,71	0,001	↑ D7	Sugar	?
	M235T592	0,861	9,86	0,01	↑ M3	3-Hydroxybutyric acid	92%
D7 vs M12							
	M246T847	1,076	14,12	<0.0001	↑ M12	Ribonic acid	85%
	M285T827	1,063	13,78	<0.0001	↑ M12	Cis aconitic acid	86%
	M231T736	1,04	12,26	<0.0001	↑ M12	?	82%
	M254T678	1,02	11,3	<0.0001	↑ M12	Characterized by the ions 254;284;299	
	M233T592	1,008	9,86	<0.0001	↑ M12	3-Hydroxybutyric acid	92%
	M42T443	1,005	7,38	<0.0001	↑ D7	Characterized by the ions 57,100,144,188,203	
	M237T845	0,982	14,08	<0.0001	↑ M12	Sugar(Pentose?)	91%
	M247T668	0,937	11,13	<0.001	↑ M12	?	
	M117T809	0,928	13,48	0	↑ M12	Sugar (Hexose?)	83%
	M103T946	0,916	15,76	<0.0001	↑ D7	D-Glucose	91%

VIP :Variable importance on projection

p   :p value

D7: The 7th day post-transplantation, M3: 3 months after transplantation, M12: 12 months after transplantation

872

873

874

875

Table 4: Metabolites that were differentially expressed over time in urines of patients.

Compound	Analytical Method	Overrepresented at time "T"	Main pathway description*
Acetic acid	1H NMR	M3 and M12	Taurine and hypotaurine metabolism
Acetoacetic acid	1H NMR	M3 and M12	Synthesis and degradation of ketone bodies
L-Alanine	1H NMR	D7	Taurine and hypotaurine metabolism
Citric acid	1H NMR	M3 and M12	Citrate cycle (TCA)
cis-Aconitic acid	GC-MS	M12	Citrate cycle (TCA)
Dihydroxyacetone	1H NMR	M3 and M12	Dimethylamine metabolism
3-Hydroxybutyric acid	GC-MS	M3 and M12	Synthesis and degradation of ketone bodies
Dimethylamine	1H NMR	D7	Dimethylamine metabolism
Myoinositol	GC-MS	D7	Galactose metabolism/ Inositol phosphate metabolism
Formic acid	1H NMR	M3 and M12	Dimethylamine metabolism
D-Glucose	GC-MS	D7	Glycolyse
Hippuric acid	1H NMR	M3 and M12	Phenylalanine metabolism
N-methylnicotinamide	1H NMR	M3 and M12	Nicotinamide metabolism
Alpha-N-Phenylacetyl-L-Glutamine	1H NMR	M3 and M12	Phenylalanine metabolism
N-methyl-2-pyridone-5-carboxamide (2PY)	1H NMR	M3	Nicotinamide metabolism
Ribonic acid	GC-MS	M12	Pentoses metabolism
Succinic acid	1H NMR	M3	Citrate cycle (TCA)
Taurine	1H NMR	D7	Taurine and hypotaurine metabolism
Trimethylamine	1H NMR	D7	Dimethylamine metabolism
Trimethylamine N-oxide	1H NMR	D7	Dimethylamine metabolism
Tyrosine	1H NMR	M3 and M12	Phenylalanine metabolism

* according to MetPA web-based tool. The more relevant is indicated in case the metabolite also hits in a secondary pathway

D7: The 7th day post-transplantation,M3: 3 months after transplantation,M12: 12 months after transplantation

876

877

878

879

880

Table 5 : Results from pathway analysis with MetPA, restricted to those with more than one hit or with impact > 0.1

Pathway	Total	Expected	Hits	Raw p	- LN(p)	Holm-Bonferoni p	FDR	Impact
Dimethylamine and methane metabolisms	34	0,30	5	7,18E-06	11,84	5,75E-04	5,75E-04	0,16
Phenylalanine metabolism	45	0,39	4	5,06E-04	7,59	4,00E-02	1,52E-02	0,03
Citrate cycle (TCA)	20	0,17	3	5,94E-04	7,43	4,63E-02	1,52E-02	0,13
Dicarboxylate metabolism	50	0,44	4	7,60E-04	7,18	5,86E-02	1,52E-02	0,15
Synthesis and degradation of ketone bodies	6	0,05	2	1,07E-03	6,84	8,09E-02	1,70E-02	0,70
Butanoate metabolism	40	0,35	3	4,60E-03	5,38	3,40E-01	5,25E-02	0,06
Taurine and hypotaurine metabolism	20	0,17	2	1,25E-02	4,38	9,15E-01	1,25E-01	0,33
Tyrosine metabolism	76	0,66	3	2,67E-02	3,62	1,00E+00	2,23E-01	0,05
Pyruvate metabolism	32	0,28	2	3,07E-02	3,48	1,00E+00	2,23E-01	0,10
Propanoate metabolism	35	0,31	2	3,63E-02	3,32	1,00E+00	2,42E-01	0,03
Inositol Phosphate metabolism	39	0,34	1	2,91E-01	1,23	1,00E+00	9,53E-01	0,14

Total :is the total number of compounds in the pathway

Hits :is the actually matched number from the user uploaded data

Raw p: is the original p value calculated from the enrichment analysis

Holm p: is the p value adjusted by Holm-Bonferroni method

FDR p :is the p value adjusted using False Discovery Rate

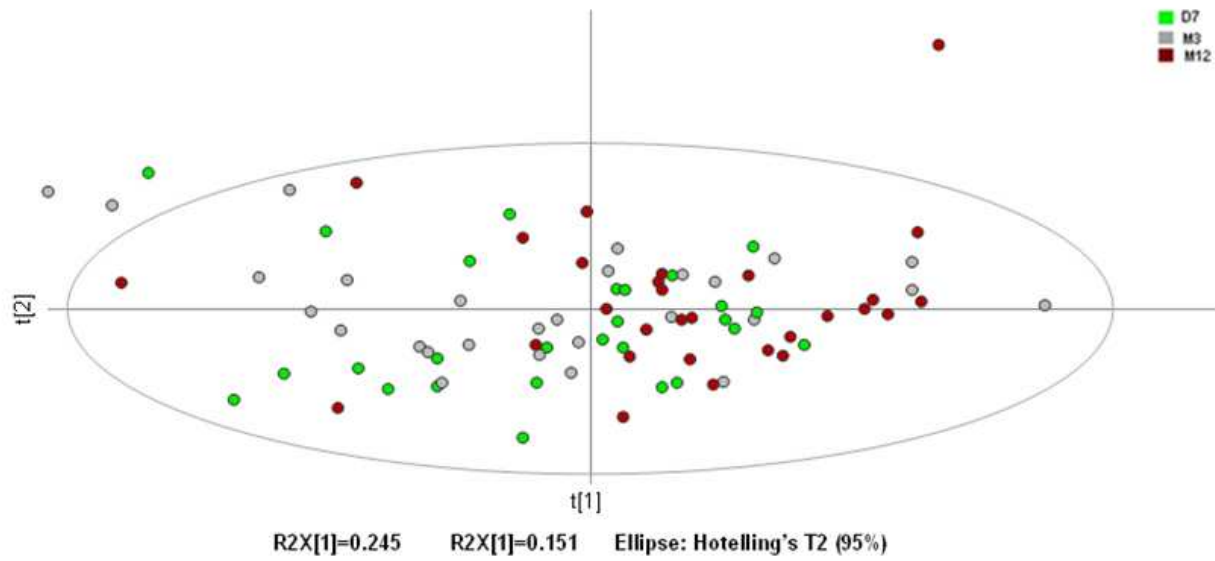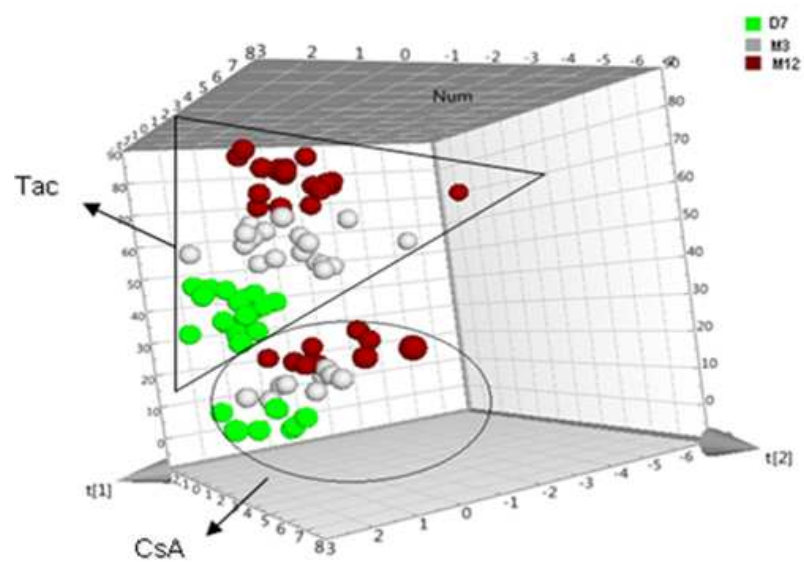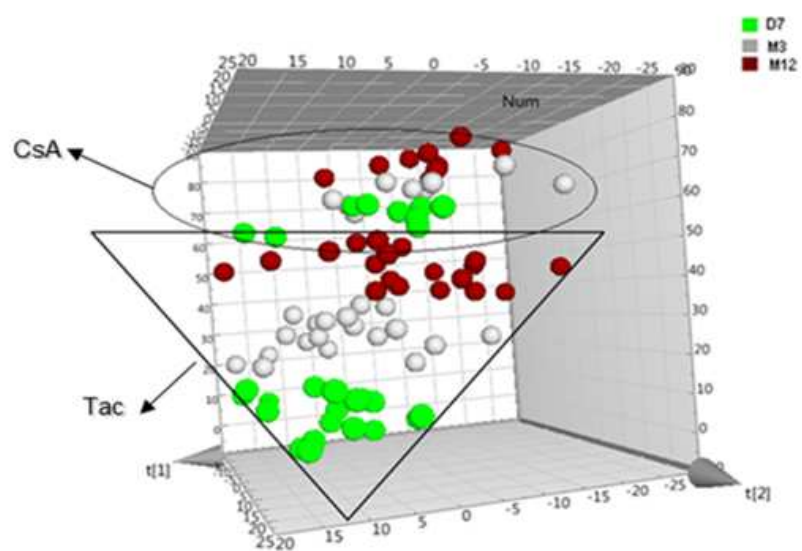Impact :is the pathway impact value calculated from pathway topology analysis

881

882

883

884

885

886

887

888

Table 6 : Results from pathway analysis with MetPA when analyzing separately the metabolites at each sampling time, restricted to those significantly over-represented or with impact > 0.1

Pathway	Total	Expected	Hits	Raw p	- LN(p)	Holm-Bonferroni p	FDR	Impact
Impacted at D7								
Dimethylamine and methane metabolism	34	0,10	3	8,68E-05	9,35	6,94E-03	6,94E-03	0,00
Taurine and hypotaurine metabolism	20	0,06	2	1,35E-03	6,61	1,06E-01	5,38E-02	0,36
Galactose metabolism	41	0,12	2	5,63E-03	5,18	1,45E-01	2,25E-01	0,00
Inositol phosphate metabolism	39	0,11	1	1,08E-01	2,23	1,00E+00	9,95E-01	0,14
Impacted at M3								
Phenylalanine metabolism	45	0,15	3	3,20E-04	8,05	2,56E-02	2,56E-02	0,03
Pyruvate metabolism	32	0,11	2	4,56E-03	5,39	3,60E-01	1,37E-01	0,10
Dimethylamine and methane metabolism	34	0,10	2	5,14E-03	5,27	4,01E-01	1,37E-01	0,16
Dicarboxylate metabolism	50	0,17	2	1,09E-02	4,52	8,31E-01	1,75E-01	0,14
Impacted at M12								
Phenylalanine metabolism	45	0,15	3	9,08E-04	7,00	7,62E-02	4,95E-02	0,03
Dicarboxylate metabolism	50	0,17	3	1,24E-03	6,69	9,78E-02	4,95E-02	0,15
Citrate cycle (TCA)	20	0,09	2	3,45E-03	5,67	2,69E-01	9,20E-02	0,12
Pyruvate metabolism	32	0,15	2	8,74E-03	4,74	6,30E-01	1,57E-01	0,10
Dimethylamine and methane metabolism	34	0,16	2	9,84E-03	4,62	7,48E-01	1,57E-01	0,16
Synthesis and degradation of ketone bodies	6	0,03	1	2,71E-02	3,61	1,00E+00	3,10E-01	0,70

D7: The 7th day post-transplantation,M3: 3 months after transplantation,M12: 12 months after transplantation

Total :is the total number of compounds in the pathway

Hits :is the actually matched number from the user uploaded data

Raw p: is the original p value calculated from the enrichment analysis

Holm p: is the p value adjusted by Holm-Bonferroni method

FDR p :is the p value adjusted using False Discovery Rate

Impact :is the pathway impact value calculated from pathway topology analysis

889

890

891

892

1-a

R2X[1]=0.251   R2X[1]=0.176   Ellipse: Hotelling's T2 (95%)

1-b

R2X[1]=0.245   R2X[1]=0.151   Ellipse: Hotelling's T2 (95%)
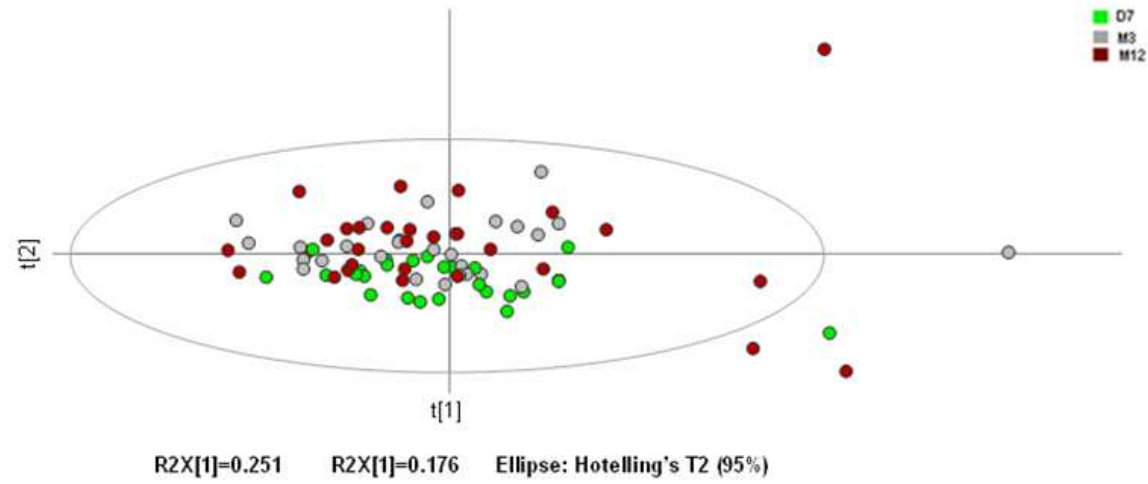
1

1

2-a

R2X[1]=0.152   R2X[2]=0.123

2-b

R2X[1]=0.205   R2X[2]=0.116

2

2

3

3

4

5-a

5-b

5

6

7

8-a

R2X[1]=0.307   R2X[2]=0.232
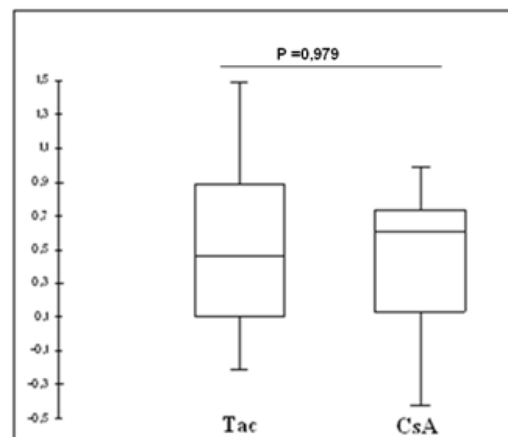
8-b
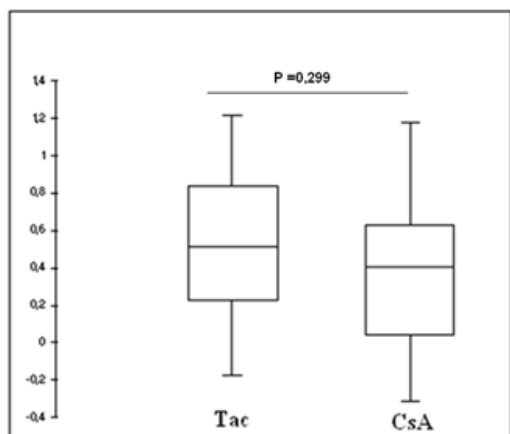
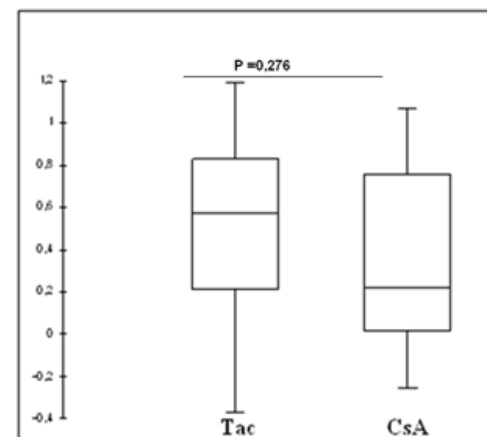R2X[1]=0.433   R2X[2]=0.208

8

9

9

10-a

10-b

10-c

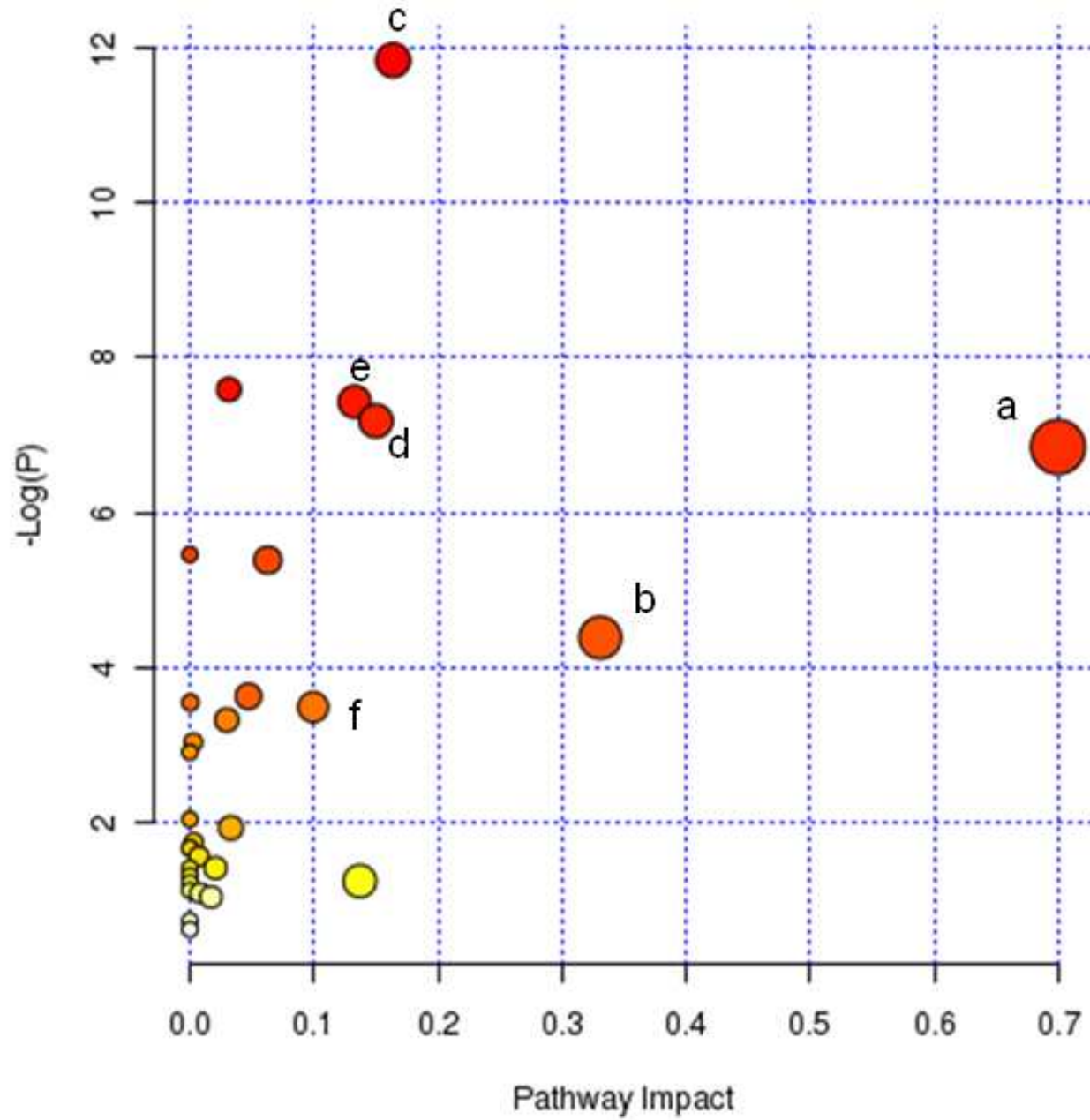10-d

10
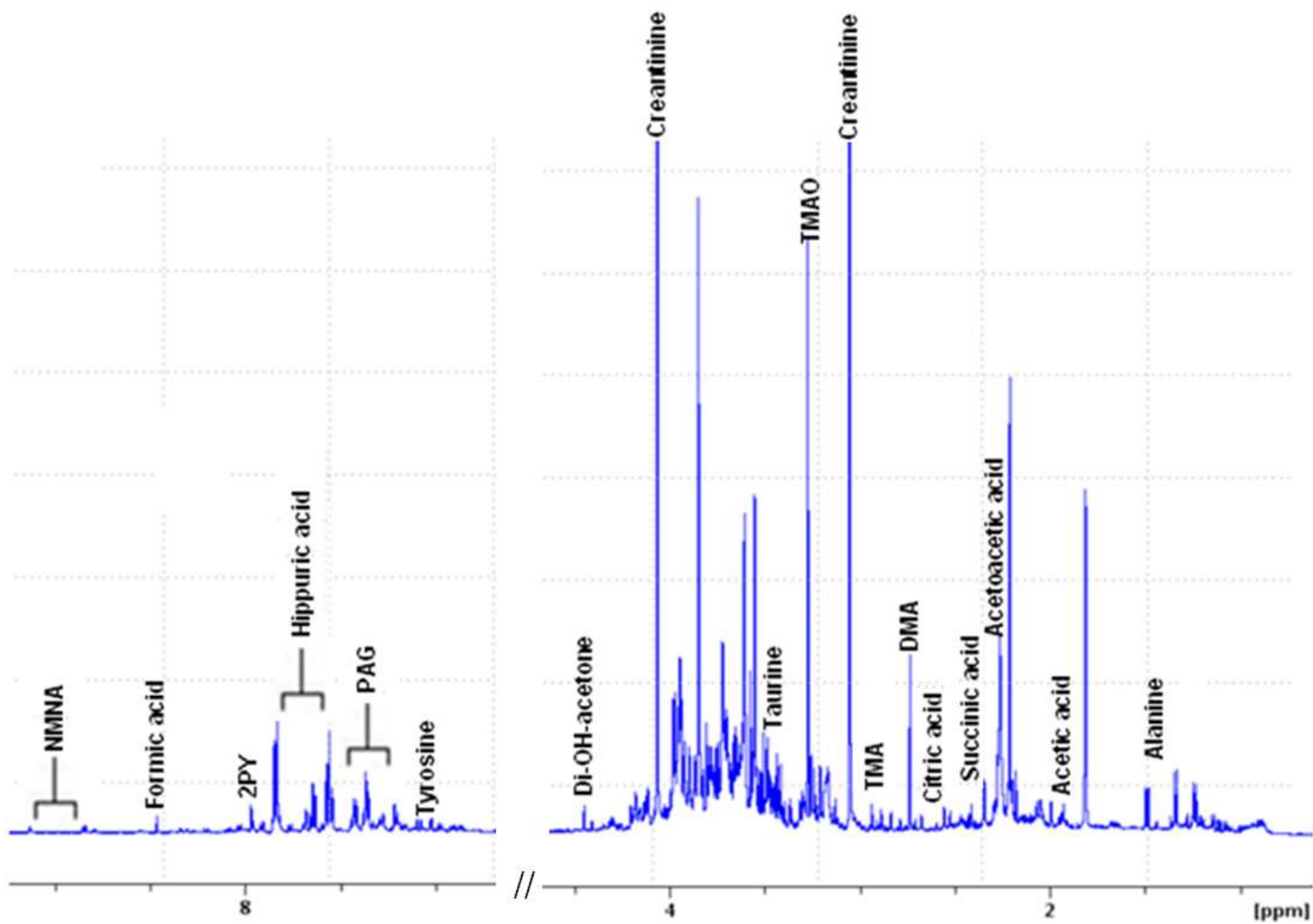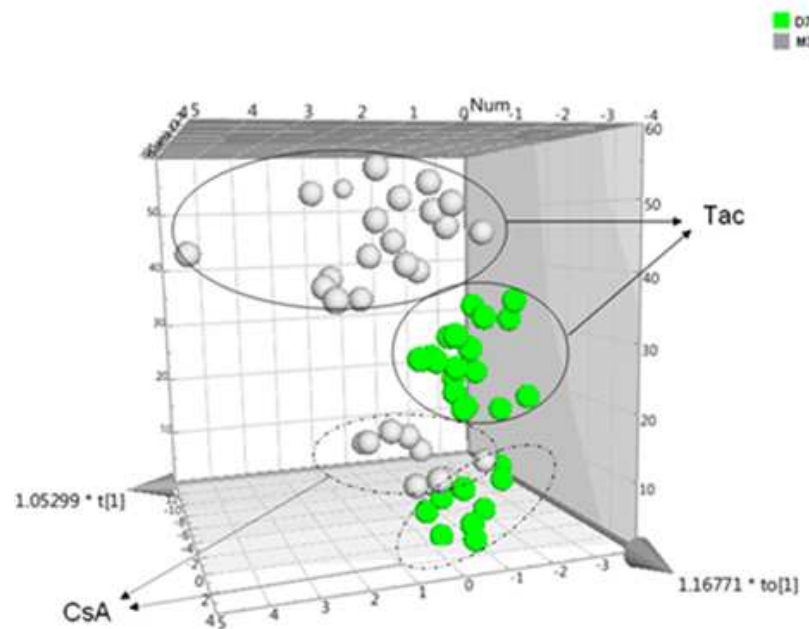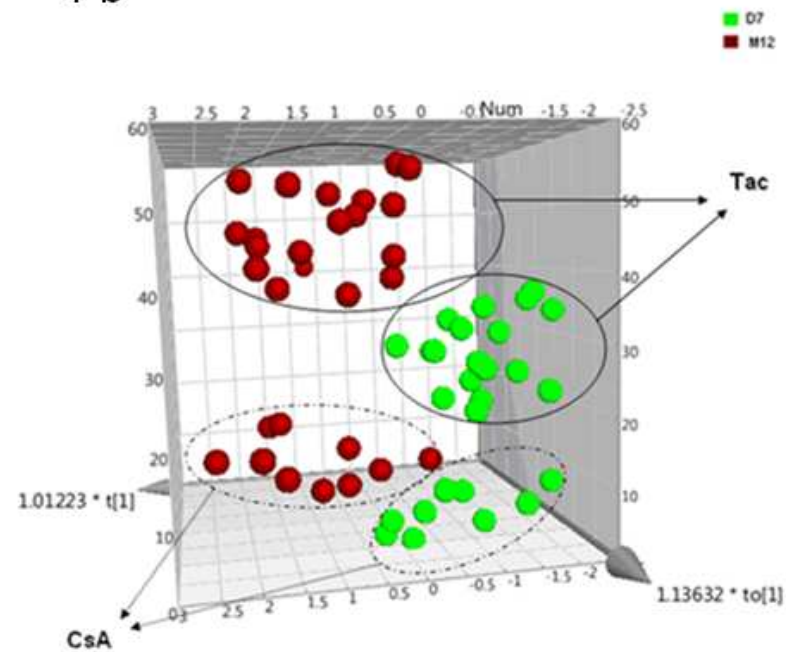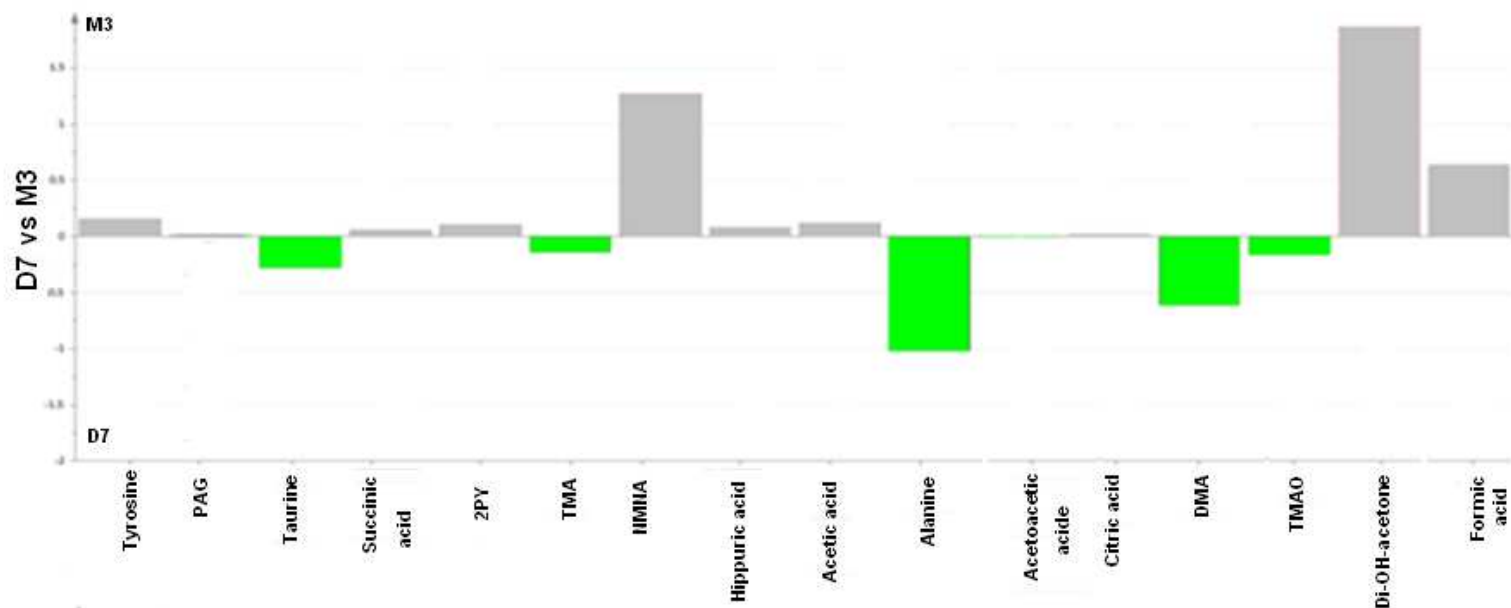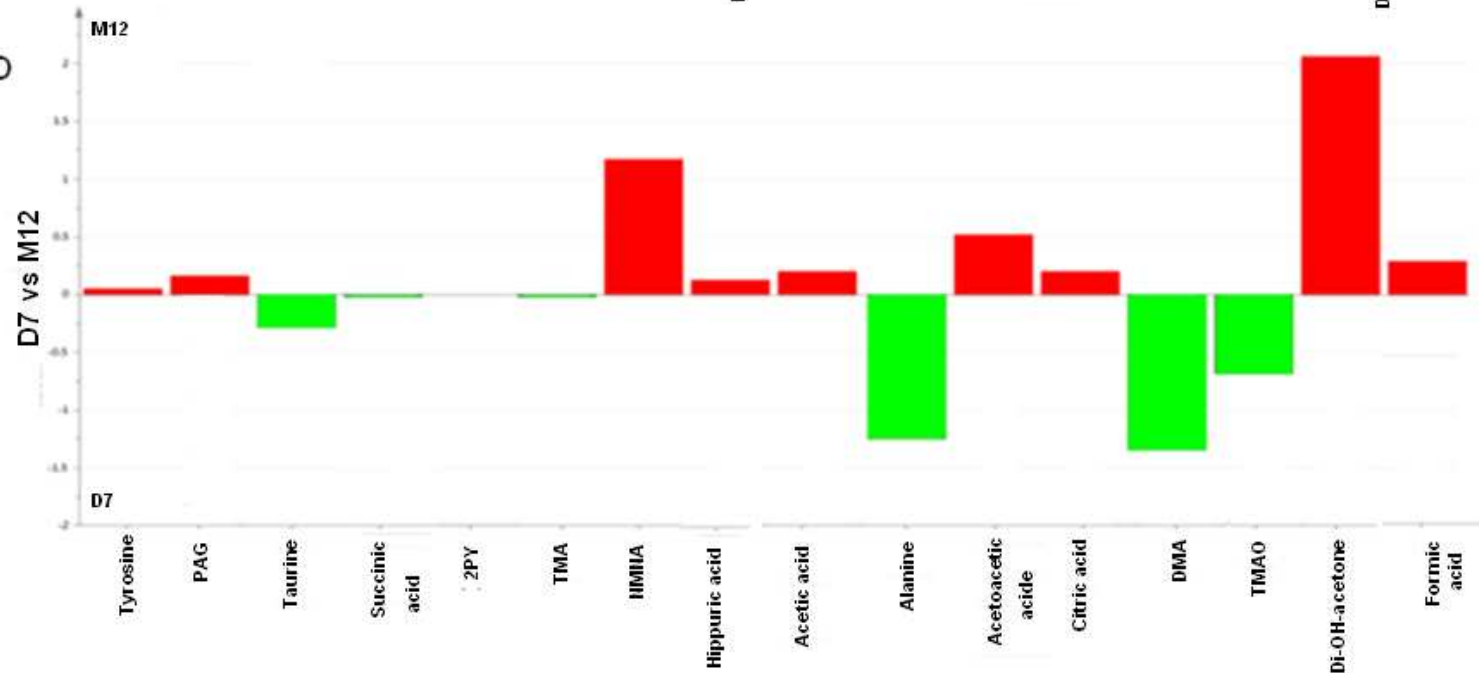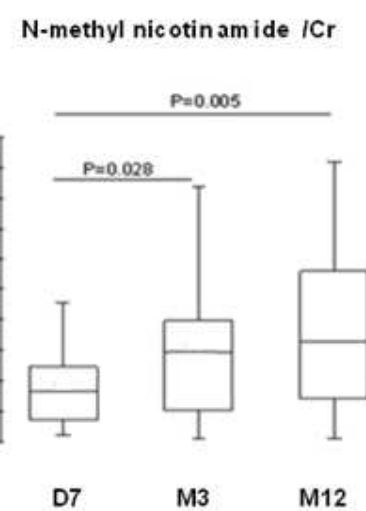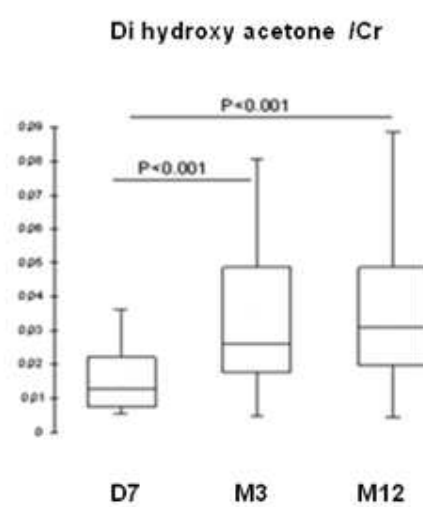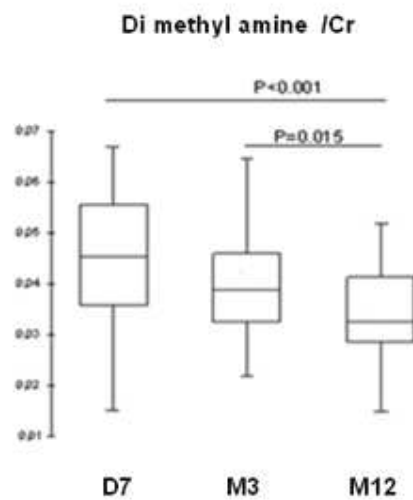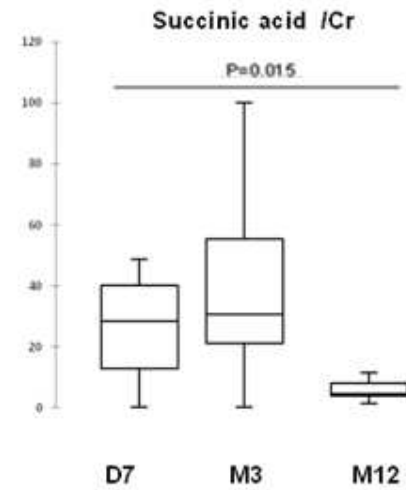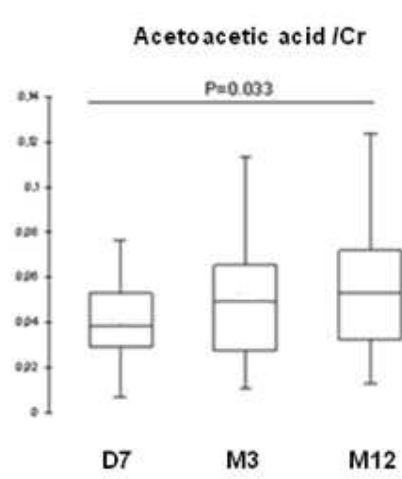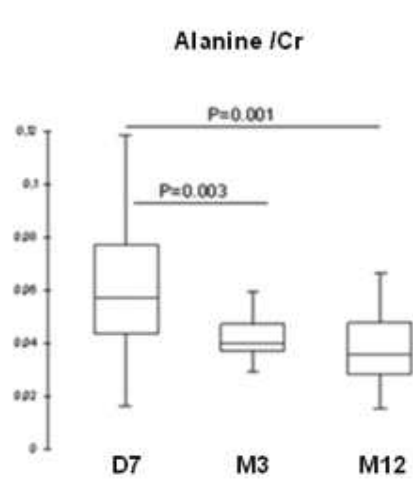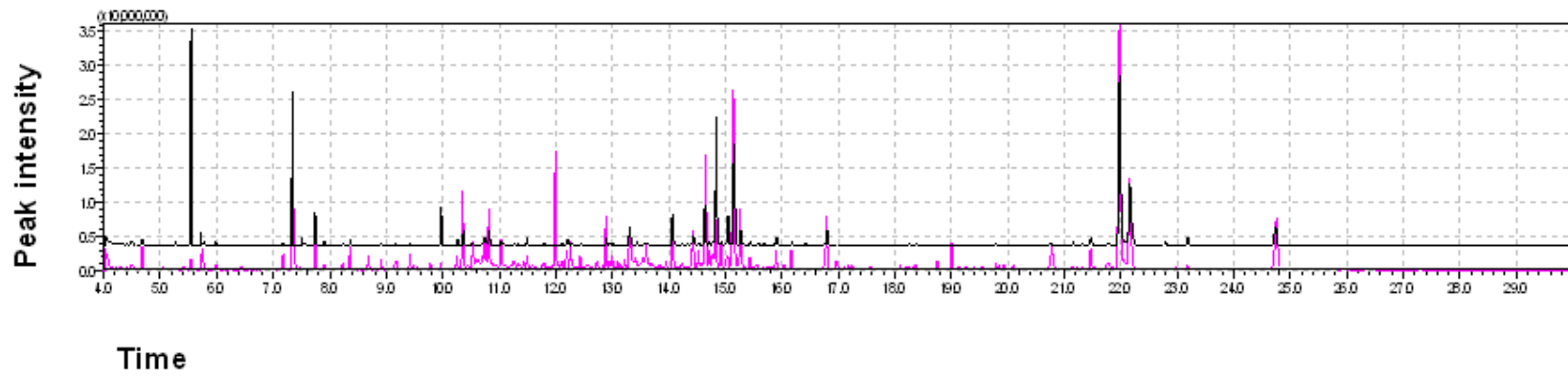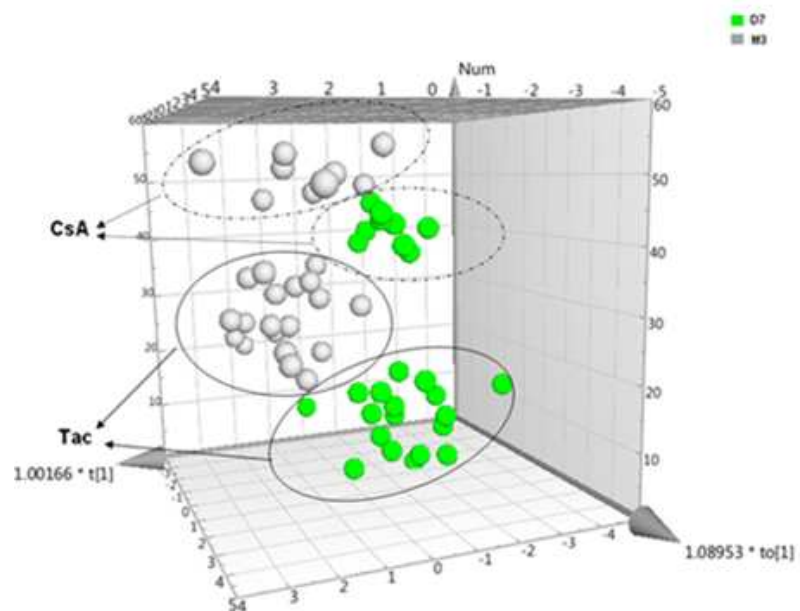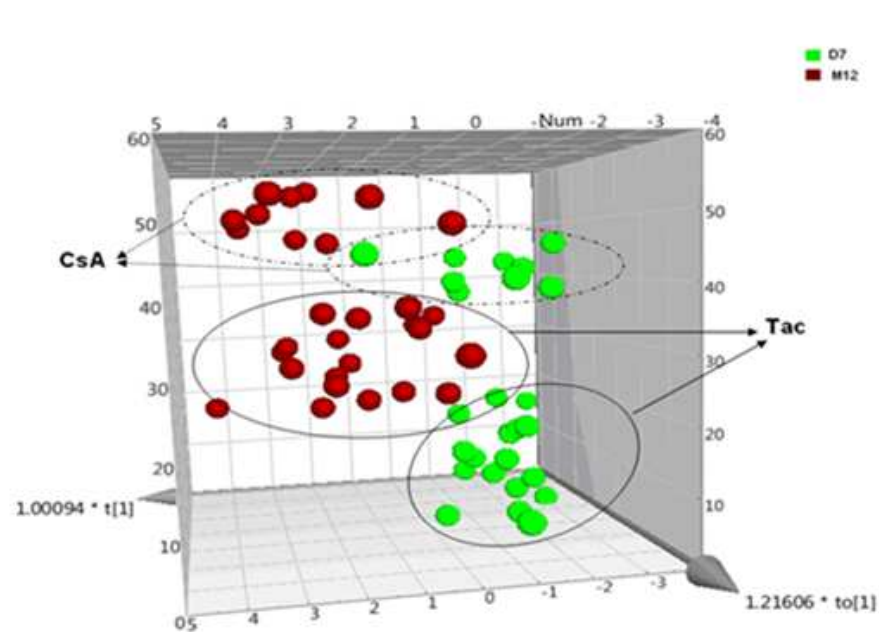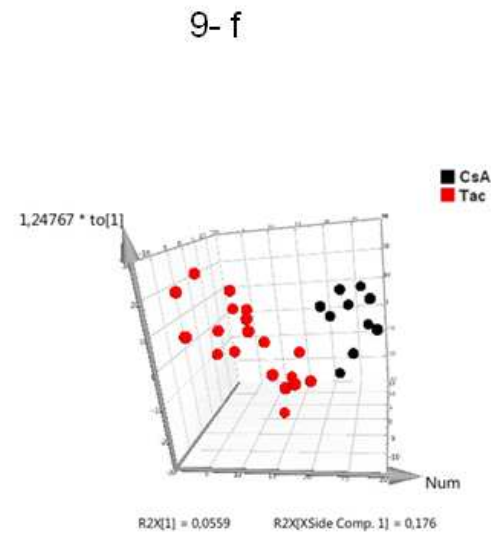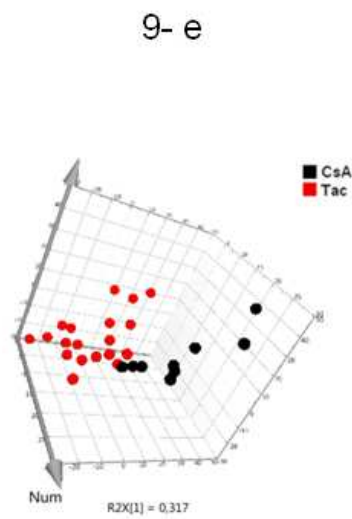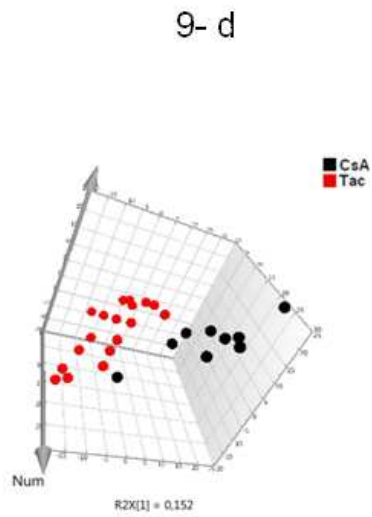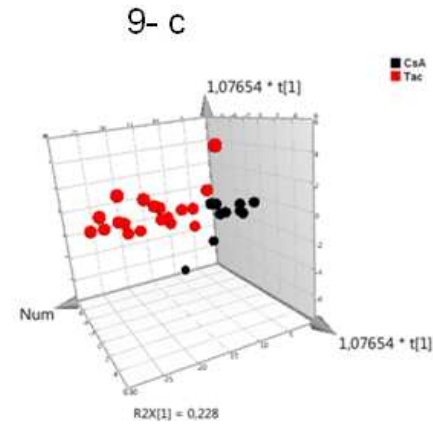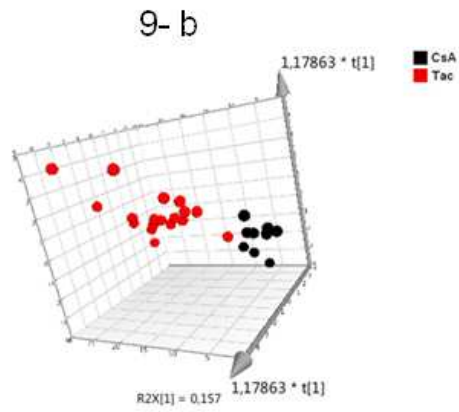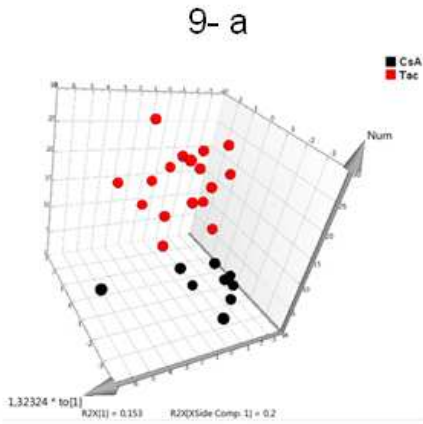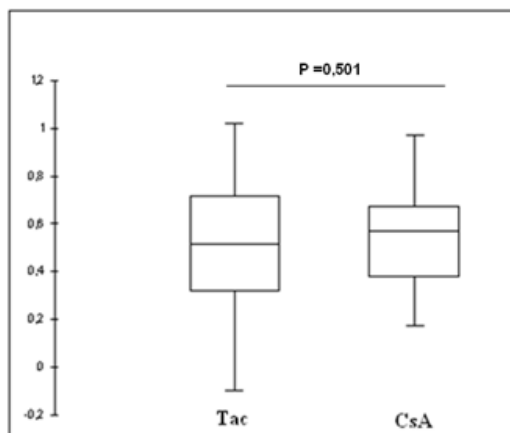
Metabolites	Synthesis and degradation of ketone bodies	Taurine and hypotaurine metabolism	Dimethylamine and methane metabolisms	Citrate cycle	dicarboxylate metabolism	Phenylalanine metabolism	inositol phosphate metabolism	Glycolysis	Nicotinamide metabolism	Pentose metabolism	Butanoate metabolism	Alanine, aspartate and glutamate metabolism	Tyrosine metabolism	Pyruvate metabolism	Propanoate metabolism
Acetic acid		M3 M12												M3 M12	
Acetoacetic acid	M3 M12										M3 M12		M3 M12		M3 M12
L-Alanine		D7										D7			
Citric acid				M3 M12	M3 M12										
Cis-aconitic acid				M12	M12										
Dihydroxyacetone				M3 M12											
3-Hydroxybutyric acid	M3 M12										M3 M12				
Dimethylamine			D7												
Myoinositol							D7								
Formic acid			M3 M12		M3 M12									M3 M12	
D-Glucose								D7							
Hippuric acid						M3 M12									
N-methyl-nicotinamide									M3 M12						
Alpha-N-Phenylacetyl-L-glutamine						M3 M12									
N1-Methyl-2-pyridone-5-carboxamide									M3						
Ribonic acid										M12					
Succinic acid				D7							D7	D7	D7		D7
Taurine		D7													
Trimethylamine			D7												
Trimethylamine N-oxide			D7												
Tyrosine						M3 M12							M3 M12		

12

13

14

15

16

17

18

19

20

21

22

23

24

25

13

26